HIV-1 Envelope glycoprotein modulates CXCR4 clustering and dynamics on the T cell membrane

Adriana Quijada-Freire[1], César A. Santiago[2], Eva M. García-Cuesta[1], Blanca Soler-Palacios[1], Rosa Ayala-Bueno[1], Sofía R. Gardeta[1], Enara San Sebastian[3], Eva Armendariz-Burgoa[4], María C. Puertas[4], Ricardo Villares[1], Urtzi Garaigorta[3], Luis Ignacio González-Granado[5,6], José Miguel Rodríguez-Frade[1], Jakub Chojnacki[4,7,8], Javier Martinez-Picado[4,7,9,10], Mario Mellado[1*]

[1]Chemokine Signaling group, Department of Immunology and Oncology, Centro Nacional de Biotecnología/CSIC, Campus de Cantoblanco, 28049, Madrid, Spain

[2]X-ray Crystallography Unit, Department of Macromolecules Structure, Centro Nacional de Biotecnología/CSIC, Campus de Cantoblanco, 28049, Madrid, Spain

[3]Departamento de Biología Molecular y Celular, Centro Nacional de Biotecnología/CSIC Campus de Cantoblanco, 28049, Madrid, Spain.

[4]IrsiCaixa, 08916, Badalona, Spain.

[5]12 de Octubre Health Research Institute (imas12), E-28012 Madrid, Spain.

[6]Department of Public Health School of Medicine, School of Medicine Universidad Complutense de Madrid, E-28040 Madrid, Spain.

[7]CIBERINFEC, 28029, Madrid, Spain

[8]Germans Trias i Pujol Research Institute (IGTP), 08916, Badalona, Spain

[9]University of Vic-Central University of Catalonia, 08500, Vic, Spain

[10]Catalan Institution for Research and Advanced Studies (ICREA), 08010 Barcelona, Spain.

[*]Corresponding author: Mario Mellado, Department of Immunology and Oncology, CNB/CSIC, Darwin 3, Cantoblanco, 28049 Madrid Spain. Tel: (+34) 91/585-4852; Fax: (+34) 91/372-0493; e-mail: mmellado@cnb.csic.es

Abstract

HIV-1 entry into susceptible cells requires the dynamic interaction of its envelope (Env) glycoprotein with the host cell receptor CD4 and a co-receptor, either CCR5 or CXCR4. While the core molecular mechanisms driving Env-receptor interactions and subsequent membrane fusion are well characterized, the precise nanoscale spatial reorganization of these co-receptors at the viral binding site remains poorly defined. In this study, we employed single-particle tracking total internal reflection fluorescence (SPT-TIRF) microscopy to quantitatively analyze nanoscale organizational changes of CXCR4 on the surface of $CD4^+$ T cells following binding by X4-tropic HIV-1. Our data reveal that both recombinant X4-gp120 and virus-like particles expressing physiological levels of X4 Env proteins (gp120 and gp41) promote CXCR4 clustering, a phenomenon linked to cell infection. Furthermore, these ligands induced oligomerization of $CXCR4^{R334X}$, a naturally occurring mutant associated with WHIM syndrome that supports HIV-1 infection but fails to oligomerize in response to CXCL12. Our findings establish a link between CXCR4 clustering and HIV-1 infection, enhancing our understanding of the initial events in viral attachment and entry. These results further suggest that HIV-1 depends on a specific spatial arrangement of co-receptors, distinct from that induced by their natural chemokine ligands, highlighting the critical role of cell-surface receptor spatial organization in dictating cellular function.

Introduction

HIV-1 infects immune cells through a dynamic interaction between its envelope glycoprotein complex (Env), composed of gp41 and gp120 trimers (1, 2), and two receptors on target cells: the primary receptor CD4, and a co-receptor, either CCR5 or CXCR4. These co-receptors are critical for viral entry and determine viral tropism. R5 strains (M-tropic) infect primary macrophages and certain memory $CD4^+$ T cells by binding to CD4 and CCR5(3), while X4 strains (T-tropic) infect primary $CD4^+$ T cells by binding to CD4 and CXCR4 (4).

R5-tropic viruses are typically the primary mode of transmission in humans and remain prevalent throughout the infection (5). However, in many infected individuals, the virus evolves its tropism over time, progressing from R5-tropic to dual-tropic (R5/X4), and ultimately to X4-tropic as the infection advances (6). This shift in tropism is associated with a more rapid decline in $CD4^+$ T cell counts (7). Furthermore, CXCR4 has been implicated in the infection of hematopoietic progenitor cells, potentially contributing to the establishment of long-lasting latent HIV-1 reservoirs (8).

The fusion of viral and cellular membranes is initiated by the binding of gp120 to CD4 (9, 10), which triggers a conformational change in gp120 that facilitates co-receptor engagement (11). These structural changes expose the N-terminal hydrophobic fusion peptide of gp41, which inserts into the cell membrane (12) to establish a fusion pore and release the viral contents into the target cell.

Numerous structural and biophysical studies have examined the HIV-1 infection process, successfully clarifying the structural requirements and conformational changes in gp120 and gp41 that enable membrane fusion and viral entry (13–16). Early investigations into host cell components revealed that HIV-1 infection induces the redistribution of cell-surface CD4 and co-receptors to the sites of viral attachment (17,

74 18). More recent evidence, obtained through super-resolution microscopy, demonstrates
75 that HIV-1 binding triggers CD4 clustering, a phenomenon also observed (albeit to a
76 lesser degree) following stimulation with gp120 alone (19). However, less is known about
77 which specific co-receptors are also recruited to the virus particles bound to the cell
78 surface. It is known that gp120 can mediate the association of CD4 with both CXCR4
79 and CCR5 (17, 20, 21). Furthermore, it has been shown that the co-expression of CCR5
80 modifies the conformation of both CXCR4 homodimers and CD4/CXCR4 heterodimers.
81 This conformational change prevents the binding of gp120 from an X4 HIV-1 strain,
82 specifically $gp120_{IIIB}$, to the resulting CD4/CXCR4/CCR5 complex (22).

83 Large-scale molecular assemblies at the cell membrane, often termed signaling
84 clusters or nanoclusters, are increasingly recognized as key regulators of cell signaling
85 (23). Evidence indicates that the spatial reorganization and distribution of membrane
86 receptors are key to controlling cell functions. Notably, clustering also appears to be
87 essential for viral infection. For instance, Env–CD4 complexes form clusters and ring-
88 like structures, facilitating closer contact between opposing membranes (24). These
89 clusters often govern a significant portion of the overall signaling process and are
90 frequently associated with the cytoskeleton (23). For example, CD4 receptors exist in pre-
91 clustered structures that enlarge upon T cell activation, thereby modulating the strength
92 of the signaling response (25, 26). Moreover, CXCR4 is organized at the cell membrane
93 as monomers, dimers and small aggregates (groups of ≥3 receptors) called nanoclusters.
94 The binding of its specific ligand, CXCL12, leads to a decrease in the proportion of
95 monomers/dimers, while simultaneously increasing the formation of larger nanoclusters.
96 This change in receptor organization consequently alters the lateral mobility of CXCR4
97 within the cell membrane (27). This mechanism is critical for initiating CXCR4 signaling
98 and enabling cells to accurately orient themselves in response to CXCL12 gradients (28).

99 A naturally occurring CXCR4 mutant, $CXCR4^{R334X}$, which is responsible for WHIM
100 syndrome, a severe immunological disorder (29), fails to form these large nanoclusters
101 upon CXCL12 binding. Consequently, cells carrying this mutation lose their ability
102 to properly sense chemoattractant gradients (28).

103 Here, we employed quantitative single-particle tracking in total internal
104 reflection fluorescence (SPT-TIRF) microscopy to directly investigate the spatial
105 arrangement and dynamic activity of CXCR4 upon exposure to HIV-1 glycoproteins.
106 Our findings reveal that both recombinant X4-gp120 and virus-like particles (VLPs)
107 containing a limited number of X4 Env proteins (gp120 and gp41) promote CXCR4
108 clustering on cells expressing CD4 and CXCR4. Moreover, they trigger the
109 oligomerization of $CXCR4^{R334X}$. These results suggest that, along with CD4
110 clustering, the conformational changes in chemokine receptors triggered by HIV-1 are
111 essential for cell infection and differ from the effects of the natural ligand, CXCL12.
112 Therefore, CD4/CXCR4 complexes and their interaction sites represent potentially
113 valuable targets for developing novel therapeutic strategies to block HIV-1 entry.

114
115

116

117 **Materials and methods**

118 ***Cells and reagents***

119 HEK-293T cells, Jurkat human leukemia cells (JKCD4$^-$X4$^+$), and Daudi cells were
120 obtained from the American Type Culture Collection (CRL-3216, CRL-10915 and
121 CCL- 213, respectively; ATCC, Rockville, MD). HEK-293CD4 cells, Jurkat CD4$^+$ cells
122 (JKCD4$^+$X4$^+$), and Jurkat cells expressing an X4-tropic HIV-1 Env (JKHXBC2) were
123 kindly provided by Drs. G. del Real (Instituto Nacional de Investigación y Tecnología
124 Agraria y Alimentaria, Madrid, Spain) and J. Alcamí (Centro Nacional de Microbiología,
125 Instituto de Salud Carlos III, Madrid, Spain). Where indicated, Jurkat cells lacking
126 endogenous *CXCR4* (JKCD4$^+$X4$^-$) (30) were electroporated with plasmids expressing
127 wild-type CXCR4-AcGFP or mutant CXCR4^{R334X}-AcGFP receptors (20 μg), as described
128 (30). Stable Jurkat cells expressing CXCR4^{R334X} (JKCD4$^+$CXCR4^{R334X}) were generated by
129 electroporation with CXCR4^{R334X} and antibiotic selection (30).

130 Human peripheral blood mononuclear cells (PBMCs) were isolated from the
131 blood of a patient with WHIM syndrome (CXCR4^{R334X}) or from healthy donors, and
132 when required from buffy coats of healthy donors, which were obtained from the Centro
133 de Transfusiones (Comunidad Autónoma de Madrid, Spain) by centrifugation through
134 Percoll density gradients (760 × g, 45 min, room temperature [RT]). CD4$^+$ cells were
135 purified by negative selection using Dynabeads (Invitrogen, Thermo Fisher Scientific,
136 Waltham, MA) and activated *in vitro* for 1 week with 50 U/mL of IL-2 (Teceleukin;
137 Roche, Nutley, NJ) and 5 μg/mL phytohemagglutinin (Roche, Basel, Switzerland) to
138 generate T cell blasts (31). The study using blood from WHIM patients and healthy
139 donors was approved by the Institutional Review Board of the 12 de Octubre Health
140 Research Institute (Nº CEIm: 24/248), and was conducted according to the principles of
141 the Declaration of Helsinki. Informed consent was obtained from all patients.

142 Recombinant gp120 protein, HXBc2, was obtained from MyBiosource
143 (#MBS43404, MyBiosource Inc., San Diego, CA). The following antibodies were used:
144 anti-human CXCR4 monoclonal antibody (mAb) (clone 44717) and phycoerythrin-
145 conjugated anti-human CXCR4 mAb (clone 12G5; both from R&D Systems,
146 Minneapolis, MN); goat F(ab')2 anti-mouse IgG-PE (Southern Biotech, Birmingham,
147 AL); anti-human CD4 mAb (clone OKT4; Biolegend, San Diego, CA); anti-histidine
148 mAb (clone AD1.1.10; R&D Systems); rabbit anti-$gp120_{IIIb}$ Ab (32); rabbit anti-Gag p24
149 HIV-1 mAb (R&D Systems); and anti-phospho-AKT mAb (S473; #4060), anti-phospho-
150 ERK1,2 mAb (T202/Y204; #9191), and anti-phospho-Lck mAb (Y505; #2751) (all from
151 Cell Signaling Technology, Danvers, MA); anti-tubulin mAb conjugated with rhodamine
152 (Bio-Rad, Hercules, CA); phalloidin-TRITC (#P1951, Sigma-Merck, St Louis, MO);
153 anti-ICAM 3 mAb (clone HP2/19) kindly donated by Dr. Francisco Sánchez Madrid
154 (Instituto Sanitario Hospital Universitario La Princesa); goat anti-mouse-AF488 Ab
155 (Thermo Fisher Scientific); anti-human gp120 mAb Fab fragments (clone 2G12;
156 Polymun Scientific, Vienna, Austria); anti-human IgG Fab fragments (Jackson
157 ImmunoResearch, West Grove, PA) conjugated to Abberior STAR RED (Abberior
158 GmbH, Gottingen, Germany), kindly donated by Dr. Jakub Chojnacki (Germans Trias i
159 Pujol Research Institute (IGTP)); anti-p24 HIV-1 (clone 37G12; Polymun Scientific)
160 conjugated with Abberior STAR ORANGE. Human CXCL12 was obtained from
161 PeproTech (Rocky Hill, NJ), and human CXCR4 was cloned into the pAcGFPm-N1
162 plasmid (Clontech Laboratories, Palo Alto, CA), as described (33).

163 Fab fragments for staining in stimulated emission depletion (STED) microscopy
164 were generated from the respective IgGs using the Fab Micro Preparation 3 Kit (Pierce,
165 Thermo Fisher Scientific). The quality of Fab preparations was determined by measuring
166 the absorbance of the eluted fractions of each conjugated antibody (at 280 nm and at the

167 wavelength of maximum absorption of the fluorochrome). Anti-human Fab fragments
168 were coupled to Abberior STAR RED dye *via* NHS-ester chemistry according to the dye
169 manufacturer's instructions.

170 CellTracker Orange CMTMR and Blue CMAC (#C2927 and #C2110,
171 respectively) were from Thermo Fisher Scientific.

172 ***Gene constructs***

173 Genes of HIV-1 gp120 (residues 31-507) from the isolate HXB2 (HIV-1_{IIIB}), with a C-
174 terminal 6×histidine tag, were amplified by PCR from pHXB2-env (#1069 NIH-AIDS
175 Reagent Program) using the oligonucleotides 5'NheI (5' TAACCGGTGCCAC
176 CATGGACAGAGCCAAGCTGCTGCTGTTGCTGCTGCTGCTGCTGCTGCCTCAG
177 GCTCAGGCCACTGAGAAGCTGTGGGTG 3') and 3'NotI (5' ATGCGGCCGCTCA
178 GTGATGGTGATGGTGATGGGATCCACGCGGAACCAGCTGCACCACTCTTCT
179 3'), and were cloned into pIRES-PURO3 (#631619 from Clontech Laboratories).

180 The CD4 extracellular domain (residues 1-388), with a C-terminal 6×histidine tag,
181 was amplified by PCR from CD4-pcDNA-3.1, kindly donated by Dr. Santos Mañes
182 (Centro Nacional de Biotecnología, CSIC) (34) using the oligonucleotides 5'AgeI (5'
183 TAACCGGTATGAACCGGGGAGTCCCT 3') and 3' NotI (5' ATGCGGCCGCCTAGTATG
184 GTGATGGTGATGCAAGTCCTCTTCAGAAATGAGCTTTTGCTCGGGCAGAACCT
185 TGAT 3'), and was cloned into pIRES-PURO3 (#631619 from Clontech Laboratories).
186 Stably-transfected HEK-293T cell lines were generated for each construct. Briefly, 0.5 ×
187 10^6 cells were seeded in DMEM supplemented with 10% FCS in a 6-well plate 24 hours
188 before transfection. Cells were then transfected with Expifectamine in OptiMem media
189 (ExpiFectamine™ 293 transfection kit; #A14525 from Thermo Fisher Scientific). At 48
190 hours post-transfection, cells were transferred to DMEM containing 10% FBS and 2
191 μg/mL puromycin for selection (1 × 10^4 cells per well in a 96-well plate). Protein
192 expression was confirmed by western blotting (using anti-gp120IIIB or anti-histidine

193 mAbs, depending on the construct). Positive clones were expanded, frozen, and stored in
194 liquid nitrogen.

195 ***Purification of recombinant proteins: soluble HIV-1 gp120 and soluble CD4***

196 HEK-293T cells expressing C-terminal his-tagged HXB2-gp120 or the extracellular CD4
197 domain were grown in DMEM containing 10% FBS and 2 μg/mL puromycin in 150-mm
198 plates. The filtered supernatants were passed through a Nickel Agarose Extrachel column,
199 Ni-NTA, (ABT technologies, Madrid, Spain) at a flow rate of 0.5 mL/min. Each
200 recombinant histidine-tagged protein was eluted utilizing a step-gradient protocol using
201 a Tris 50 mM pH 8, NaCl 500 mM buffer containing 500 mM imidazole. The elution
202 involved initial steps of 10% and 20% imidazole, followed by a linear gradient to 100%
203 to ensure complete protein recovery. The eluted fractions were analyzed by SDS-PAGE
204 gel electrophoresis. Those fractions containing the protein of interest were pooled and
205 concentrated to a final volume of 0.5 mL. The concentrated sample was subjected to gel
206 filtration chromatography using a S200 Increase (10/300) column (Cytiva, Freiburg,
207 Germany). The eluted fractions were analyzed by SDS-PAGE and fractions containing
208 the expected molecular size were pooled, aliquoted, and stored at -80ºC.

209 ***Production of viral-like particles and lentiviral particles***

210 Production of VLPs in HEK-293T cells included transfection with a plasmid encoding
211 the X4-tropic HIV-1 Env (10 μg pHXB2env; #1069 NIH-AIDS Reagent Program) and a
212 plasmid encoding a second-generation packaging system (7 μg psPAX2; #12260
213 Addgene, Watertown, MA). Supernatants were collected 48 hours post-transfection,
214 filtered through 0.45 μm filters, and clarified by ultracentrifugation (247,000 × g, 2 h,
215 4°C) on a 20% sucrose cushion, using a Beckman SW55 rotor. The resulting VLPs were
216 aliquoted and stored at -80°C. Expression of gp120 and p24 was assessed by western

217 blotting with specific antibodies. Each VLP batch was quantified using a p24 Quantikine
218 ELISA kit (R&D Systems).

219 Production of lentiviral particles (LVPs) was performed as above with the co-
220 transfection of a reporter gene (8 μg plGFP; #PS100065, OriGene, Rockville, MD)
221 instead of the double transfection. Supernatants were collected 48 hours post-transfection,
222 filtered through 0.45 μm filters, aliquoted, and stored at -80°C. Expression of gp120 and
223 p24 was assessed by western blotting with specific antibodies. Each LVP batch was
224 characterized in a transduction assay using LVPs transfected with the vesicular stomatitis
225 virus G glycoprotein (VSVG) (pCMV-VSV-G; #8454, Addgene) as a positive control.

226 ***Western blotting***

227 Cells (3×10^6) were activated with CXCL12 (50 nM) or recombinant X4-gp120 (0.3
228 μg/mL) at the time points indicated and then lysed in RIPA detergent buffer containing 1
229 mM PMSF, 10 μg/mL aprotinin, 10 μg/mL leupeptin, and 10 μM sodium orthovanadate
230 (30 min, 4ºC). Cell extracts were analyzed by western blotting using specific antibodies.
231 Densitometric evaluation of western blots was performed using ImageJ software (NIH,
232 Bethesda, MD).

233 ***Flow cytometry***

234 Cells (2×10^5/well) were incubated with specific antibodies (30 min, 4ºC) and mean
235 fluorescence intensity (MFI) was determined on a Gallios or FC500 flow cytometer
236 (Beckman Coulter). When required, Jurkat cells expressing CD4 ($JKCD4^+X4^+$ and
237 $JKCD4^+X4^-$) were incubated with X4-gp120-His (0.3 μg/mL), followed by staining with
238 an anti-histidine-PE mAb. Similarly, Daudi cells were incubated with a mixture of X4-
239 gp120 (0.3 μg/ml) and soluble hCD4-his (0.2 μg/mL), and subsequently stained with an
240 anti-histidine-PE mAb.

241 For human PBMCs, 100 μL of whole blood from healthy controls and a WHIM
242 patient were analyzed by flow cytometry for the expression of CD3-APC (IM2467),
243 CD19-PC5.5 (A66328), CD4-FITC (A07750), CD8-PC7 (737661; all from Beckman
244 Coulter Inc., Brea, CA), and CXCR4-PE (306506, Biolegend) using a Gallios flow
245 cytometer and FlowJo software.

246 Receptor internalization was evaluated after cell activation (5×10^5 cells/well)
247 with 50 nM CXCL12 or 0.3 μg/mL of recombinant X4-gp120 at the indicated time points.
248 Cells were incubated with an anti-CXCR4 mAb (clone 44717, 30 min, 4°C), followed by
249 a PE-coupled goat anti-mouse IgG (30 min, 4ºC) or, when required, with anti-CD4 (clone
250 OKT4, 20 min, 4ºC), and analyzed in a Cytoflex cytometer (Beckman Coulter). Results
251 are expressed as a percentage of mean spot intensity (MSI) of treated cells relative to that
252 of unstimulated cells.

253 To evaluate VLPs by flow cytometry, particles were coupled to latex beads (4
254 mm, 4% w/v Aldehyde/Sulfate latex; Invitrogen, Eugene, OR). After sonication (5 min,
255 RT), beads were mixed with VLPs at a ratio of 1:1 v/v (15 min, RT) in 1% casein-PBS
256 solution (Bio-Rad). Reactive groups were blocked with 100 mM glycine (60 min, 4°C,
257 with continuous rocking). Beads coupled to VLPs were washed twice by centrifugation
258 (3 min, 2000 × g) in washing buffer (PBS/BSA 0.5%), resuspended, and incubated with
259 the corresponding dilution of the recombinant soluble CD4 in casein-PBS solution (30
260 min, RT). VLP-beads conjugates were washed three times (3 min, 2,000 × g) with PBS
261 staining buffer (PBS supplemented with 2% FBS, 1% BSA, and 0.2% sodium azide) and
262 stained as above for flow cytometry.

263 ***Lentiviral particle transduction assays***

264 HEK-293 CD4 cells (1.2×10^4 cells per well in a 96-well plate) were inoculated with
265 serial dilutions of LVP-containing supernatants. Stock solutions were diluted in DMEM,

266 10% FCS, 1 mM pyruvate, and 2 mM glutamine. Sixteen hours later, the viral inoculum
267 was replaced with fresh medium and the cells were further incubated (48 h, 37°C). Viral
268 transduction efficiency was determined by GFP fluorescence analysis. The medium was
269 discarded and cells were washed with PBS and fixed using 4% formaldehyde in PBS (20
270 min, RT). Fluorescence was imaged in a Tecan Spark Cyto plate reader (Tecan Group
271 Ltd., Männedorf, Switzerland) after extensive washes with PBS. Images of 2456 × 2052
272 pixels at a 16-bit gray scale were acquired with a 4× objective. All images were captured
273 using identical exposure settings (200 ms), except for wells where cells were transduced
274 with LVPs expressing VSVG, for which an exposure time of 80 ms was used. Mean
275 fluorescence intensity of GFP signal of each image was quantitated using Fiji/ImageJ
276 v2.3.0/1.53t software.

277 ***Cell-cell fusion assay***

278 The JKHXBC2 cell line was co-cultured with the indicated Jurkat target cells at a 1:1
279 ratio in 96-well flat-bottom plates (16 h, 37°C). Prior to co-culture, each cell type was
280 stained with vital probes CellTracker Orange CMTMR and Blue CMAC, respectively.
281 Double-stained events were subsequently analyzed using a Gallios Analyzer cytometer
282 (Beckman Coulter). Results are shown as the percentage of fusion events ± SD, using as
283 a reference the fusions events detected in JKCD4$^+$CXCR4$^+$ cells.

284 ***Cell adhesion/migration on planar lipid bilayers***

285 Planar lipid bilayers were prepared as reported (35). Briefly, unlabeled GPI-linked
286 intercellular adhesion molecule 1 (ICAM-1) liposomes were mixed with 1,2-dioleoyl-
287 phosphatidylcoline. Membranes were assembled in FCS2 chambers (Bioptechs, Butler,
288 PA), blocked with PBS containing 2% FCS (60 min, RT), and coated with CXCL12 (200
289 nM, 30 min, RT) or gp120 (0.3 μg/ml, 30 min, RT). Cells (3×10^6 CD4$^+$ T blasts/mL) in
290 PBS containing 0.5% FCS, 0.5 g/L D-glucose, 2 mM $MgCl_2$, and 0.5 mM $CaCl_2$ were

291 then injected into the pre-warmed chamber (37ºC). Confocal fluorescence, differential
292 interference contrast (DIC) and interference reflection microscopy (IRM) images were
293 acquired on a Zeiss Axiovert LSM 510-META inverted microscope with a 40× oil-
294 immersion objective. Imaris 7.0 software (Bitplane, Zurich, Switzerland) and ImageJ
295 1.49v were used for qualitative and quantitative analysis of cell dynamics parameters,
296 fluorescence and IRM signals. The fluorescence signal of the planar bilayer in each case
297 was established as the background fluorescence intensity. The frequency of adhesion
298 (IRM^+ cells) per image field was estimated as [nº of cells showing IRM contact/total
299 number of cells (estimated by DIC)] × 100; similarly, we calculated the frequency of
300 migration (cells showing an IRM contract and moving over time).

301 ***STED assays***

302 Purified particles (~1 μg of p24) were adhered to glass cover slips previously coated with
303 0.01% poly-L-lysine (Sigma) for 20 minutes. Cover slips were briefly fixed with 3%
304 PFA/PBS and blocked using 2% BSA (Sigma)/PBS for 30 minutes. Particles were stained
305 for Env using 10 ng/μL 2G12 Fab fragments and anti-human Abberior STAR RED-
306 conjugated Fab fragments. Following immunostaining, particles were washed in
307 permeabilization buffer (0.1% saponin, 0.5% BSA in PBS) and stained for Gag using 20
308 ng/μL 37G12 Ab conjugated with STAR ORANGE. The samples were briefly fixed using
309 3% PFA/PBS again and were overlaid with SlowFade Diamond (Thermo Fisher
310 Scientific). All steps were carried out at RT.

311 The VLPs were imaged using an Olympus IX83 inverted confocal microscope
312 equipped with the Abberior STEDYCON STED system using a 60×/1.42NA objective.
313 The following parameters were used during STED image acquisitions: pinhole size: 1
314 Airy; dwell time: 300 μs/pixel; field of view: 20 μm × 20 μm and pixel size: 20 nm.

315 The mature state of VLPs, the percentage which express gp120 on their surface and the
316 intensity of the signal of gp120 per VLP, were quantified manually using ImageJ.

317 ***Imaging of viral-like particles by transmission electron microscopy***

318 The integrity of VLPs was examined by negative-stain electron microscopy on carbon
319 grids. Samples were incubated on the grids and were treated with 2% uranyl acetate (30
320 s, RT). Grids were examined using a transmission electron microscope (1200-EX II; Jeol,
321 Tokyo, Japan) at 100 kV, equipped with a Gatan Oneview CMOS camera.

322 ***FRET saturation curves by sensitized emission***

323 FRET analyses were performed as described (36). Briefly, HEK-293T cells (3.5×10^5
324 cells/well) were transiently transfected with cDNA encoding the fusion proteins using the
325 poly-ethylenimine method (Sigma-Aldrich). For CD4/CXCR4 or CD4/CXCR4^{R334X}
326 heterodimers, the cells were co-transfected with a fixed amount of CD4-CFP (2 μg) and
327 increasing amounts of CXCR4-YFP or CXCR4^{R334X}-YFP (0.5–8.0 μg). As a control, we
328 used a fixed amount of CD4-CFP (2 μg) and increasing amounts of 5HT$_{2B}$-YFP (0.5–12
329 μg). We incubated cells with cDNA and poly-ethylenimine (5.47 mM in nitrogen
330 residues) and 150 mM NaCl in serum-free medium, which was replaced after 4 hours by
331 complete medium. At 48 hours post transfection, cells were washed twice in HBSS
332 supplemented with 0.1% glucose and resuspended in the same solution. Total protein
333 concentration was determined for whole cells using the Bradford Assay Kit (Bio-Rad).
334 Cell suspensions (0.2 μg/μL) were added to black 96-well microplates and emission light
335 was quantified using the Wallac Envision 2104 Multilabel Reader (Perkin-Elmer,
336 Waltham, MA) as described (27). To determine FRET$_{50}$ and FRET$_{max}$ values, curves were
337 extrapolated from data using a nonlinear regression equation applied to a single binding
338 site model with a 95% confidence interval (GraphPad PRISM software, San Diego, CA).
339 When FRET at a fixed ratio was needed, HEK-293T cells were transiently co-transfected

340 with a fixed ratio of CXCR4-YFP/CD4-CFP (15 μg and 9 μg, respectively) and
341 $CXCR4^{R334X}$-YFP/CD4-CFP (9 μg and 9 μg, respectively in all cases). After 48 hours the
342 cells were treated with Env(-) VLPs (0.1 μg/mL of Gag p24) or gp120-VLPs (0.1 μg/mL
343 of Gag p24) and FRET efficiency was evaluated (n = 3, mean ± SD).

344 ***Single-molecule TIRF imaging and analysis***

345 Transfected cells expressing 8,500–22,000 receptors/cell (<4.5 particles/μm^2) were
346 selected for detection and tracking analysis. Experiments were performed at 37ºC with
347 5% CO_2 using a TIRF microscope (Leica AM TIRF inverted microscope; Leica
348 Microsystems, Wetzlar, Germany). Image sequences of individual particles (500 frames)
349 were then acquired at 49% laser power (488-nm diode laser) with a frame rate of 10 Hz
350 (100 ms/frame). The penetration depth of the evanescent field was 90 nm. Particles were
351 detected and tracked using the U-Track2 algorithm (37) implemented in MATLAB, as
352 described (27). MSI, number of mobile and immobile particles and diffusion coefficients
353 (D_{1-4}) were calculated from the analysis of thousands of single trajectories over multiple
354 cells (statistics provided in the respective figure captions) using described routines (27).
355 The receptor number along individual trajectories was determined as reported (38), using
356 the intensity of the monomeric protein CD86-AcGFP as a reference (Figure 1-Figure
357 supplement 1). Values were confirmed using single-step photobleaching analysis (27,
358 28).

359 ***HIV-1 infection in T $CD4^+$ cells of a WHIM patient***

360 All donors were female and under the age of 30. PBMCs were obtained from sero-
361 negative fresh blood of a WHIM patient and three healthy donor controls using SepMate
362 tubes (STEMCELL Technologies, Vancouver, Canada). Isolated PBMCs were cultured
363 in RPMI supplemented with 20% FBS (Gibco), 1% penicillin/streptomycin (Capricorn
364 Scientific GmbH, Ebsdorfergrund, Germany), 3 μg/mL PHA (Sigma-Aldrich), and 10

365 U/mL of IL-2 (Novartis, Basel, Switzerland) for 48 hours at 37°C. Activated PBMCs
366 were inoculated *in vitro* at a multiplicity of infection (MOI) of 0.001 with the HIV-1 NL4-
367 3 lab strain for 1 hour. After removal of the viral inoculum, cultures were split into two
368 wells and maintained in RPMI supplemented with 20% FBS, 1% penicillin/streptomycin,
369 and 10 U/mL of IL-2. Supernatants were collected at different time points and replaced
370 with fresh supplemented media. The infection rate was determined by quantification of
371 viral p24 in the supernatants using the Alliance HIV-1 p24 Antigen Elisa Kit (Perkin
372 Elmer).

373 ***Statistical analyses***

374 All results were analyzed with GraphPad Prism software version 9. Cell polarization
375 assays, using immunofluorescence or planar lipid bilayers comparing different
376 conditions, were analyzed to determine significant differences between means using one-
377 way analysis of variance (ANOVA) followed by Tukey's multiple comparisons test. Data
378 related to the percentage of mature VLPs and their surface expression of gp120 obtained
379 by STED microscopy, and MFI results by flow cytometry, were also analyzed by one-
380 way ANOVA and Tukey's multiple comparisons test. A two-tailed Mann-Whitney non-
381 parametric test was used to analyze the MFI of gp120 per VLP. The Kruskal-Wallis test
382 followed by Dunn's test was used to analyze MSI and diffusion coefficients (D_{1-4}) of
383 single particles in TIRF experiments. We used contingency tables to compare two or more
384 groups of categorical variables, such as the percentages of mobile or immobile particles,
385 and these were compared using a Chi-square test with a two-tailed p-value. Statistical
386 differences were reported as n.s. = not significant $p > 0.05$, *$p \leq 0.05$, **$p \leq 0.01$, ***p
387 ≤ 0.001 and ****$p \leq 0.0001$.

388

389 **Results**

390 **Recombinant gp120-mediated CXCR4 clustering requires CD4 expression**

391 To evaluate the role of HIV-1 in modulating CXCR4 dynamics at the cell membrane, we
392 first synthesized a recombinant X4 HIV-1 gp120 (X4-gp120) with a C-terminal histidine
393 tag to facilitate subsequent detection. We generated a HEK-293T cell line that
394 constitutively secretes the recombinant glycoprotein. The secreted X4-gp120 was isolated
395 from cell culture supernatants using a simple, rapid, non-denaturing and efficient
396 purification procedure involving Ni-NTA agarose chromatography and gel filtration
397 chromatography. The purity of the isolated glycoprotein was confirmed by SDS-PAGE
398 and western blotting, using commercial gp120 as a control and specific antibodies (Figure
399 1-Figure supplement 2A, B; Figure 1-Figure supplement 2-Source data 1, 2). The X4-
400 gp120 specifically bound to Jurkat cells expressing CD4, regardless of the presence or
401 absence of CXCR4 (JKCD4^{+}CXCR4^{+} and JKCD4^{+}CXCR4^{-}, respectively) (Figure 1-
402 Figure supplement 2C). By contrast, X4-gp120 did not bind to Daudi cells, which express
403 only CXCR4 (Figure 1-Figure supplement 2D). In this latter case, X4-gp120 binding
404 became possible when the recombinant protein was pre-incubated with soluble CD4. As
405 a control, no binding of soluble CD4 was detected in the absence of X4-gp120 (Figure 1-
406 Figure supplement 2D). These data indicate that our recombinant gp120 is a X4-tropic
407 gp120 capable of binding Jurkat cells expressing CD4.

408 Engagement of the HIV-1 Env with CD4 and/or a chemokine co-receptor activates
409 several signal transduction pathways (39, 40). For instance, gp120 binding to CD4 leads
410 to the phosphorylation of the receptor tyrosine kinase p56Lck, which then activates the
411 Raf/MEK/ERK and phosphatidylinositol 3-kinase (PI3K) pathways (41). PI3K is also
412 activated through chemokine receptor engagement (42), and only viruses capable of
413 inducing signaling *via* these receptors can establish productive infections (40). Jurkat

414 cells and primary $CD4^+$ T blasts were stimulated with X4-gp120, then lysed and analyzed
415 by western blotting. The results showed that Akt, ERK1/2 and Lck were rapidly
416 phosphorylated following X4-gp120 activation (Figure 1-Figure supplement 3; Figure 1-
417 Figure supplement 3-Source data 1, 2) in both cell types. Furthermore, it is known that
418 the interaction of gp120 with CXCR4 influences the actin cytoskeleton (43). Cytochalasin
419 D, an inhibitor of F-actin polymerization, has been shown to inhibit viral entry into
420 PBMCs (44), and to affect the formation of HIV-1 reverse transcriptase products in HeLa
421 cells (45). We thus evaluated whether X4-gp120 reorganized the actin cytoskeleton of the
422 target cells. Using artificial lipid bilayers coated with ICAM-1, we observed that both
423 CXCL12 and X4-gp120 induced the polarization of primary $CD4^+$ T blasts and,
424 furthermore, enhanced cell adhesion (Figure 1-Figure supplement 4A, B). However, only
425 CXCL12 triggered significant cell migration (Figure 1-Figure supplement 4C). These
426 findings confirmed that X4-gp120 bound CXCR4 in the presence of CD4 and was fully
427 functional on both primary $CD4^+$ T blasts and Jurkat cells.

428 The actin cytoskeleton acts as a physical barrier, influencing the
429 compartmentalization of the plasma membrane and the dynamics of membrane proteins
430 (46, 47). Consequently, the dynamic nature of actin not only defines cell shape during
431 migration, but also affects membrane organization of both CD4 (48) and CXCR4 (27).
432 Next, we transiently transfected $JKCD4^+X4^-$ cells, which express endogenous CD4, with
433 CXCR4-AcGFP. We then used SPT in TIRF-M mode to observe individual molecules
434 within the plasma membrane, allowing us to determine the effect of X4-gp120 on CXCR4
435 dynamics and stoichiometry (Figure 1-video 1-3). Consistent with previous observations
436 (27, 28), our analysis of CXCR4 dynamics in unstimulated cells revealed that the majority
437 of CXCR4 particles were mobile (~87%) (Figure 1A), exhibiting a median short time-
438 lag diffusion coefficient ($D_{1–4}$) of 0.017 $\mu m^2 s^{-1}$ (Figure 1B). Upon stimulation, both

439 CXCL12 and X4-gp120 significantly reduced the overall receptor diffusivity (CXCL12,
440 median D_{1-4} = 0.007 μm^2 s^{-1}; X4-gp120, median D_{1-4} = 0.009 μm^2 s^{-1}) (Figure 1B), and
441 increased the percentage of immobile particles from ∼13% (basal) to ∼20% (CXCL12),
442 and to ∼18% (X4-gp120) (Figure 1A). Mobile particles exhibited distinct diffusion
443 profiles, derived from mean square displacement (MSD) plots (49), and were further
444 classified based on motion using the moment scaling spectrum (50). For most mobile
445 particles (∼90% in unstimulated cells, ∼79% in CXCL12-activated cells, and ∼75% in
446 X4-gp120 stimulated cells), diffusion was confined (Figure 1-Figure supplement 5). To
447 quantify the number of receptors in individual trajectories, we measured the average
448 fluorescence intensity during the initial 20 frames of each trajectory and used the intensity
449 of the monomeric protein CD86-AcGFP as a reference (28, 51) (Figure 1-Figure
450 supplement 1). In unstimulated cells, we found a predominance of CXCR4 monomers
451 and dimers (∼98%), with only a minor fraction of oligomers, complexes containing more
452 than three receptors (∼2%). Upon the addition of saturating X4-gp120 concentrations, we
453 observed a significant reduction in the percentage of monomers and dimers (∼82%) and
454 a corresponding increase in nanoclusters composed of ≥3 receptors/particle (∼18%)
455 (Figure 1C). This observation aligns with previous findings for CXCL12 (27) As a
456 control, stimulation with CXCL12 resulted in a larger percentage of these nanoclusters
457 (∼26%) (Figure 1C). These data correlated with the higher MSI values observed after cell
458 activation (basal 933 a.u.; CXCL12 2,105 a.u., X4-gp120 1,738 a.u.) (Figure 1D).
459 Collectively, these results indicate that X4-gp120 triggers CXCR4 nanoclustering,
460 although to a lesser extent than CXCL12.

461 **gp120-expressing virus-like particles mediate CXCR4 clustering**

462 Recombinant X4-gp120 alone does not fully replicate the function of HIV-1 Env.
463 Previous studies have shown that the Env consists of gp120 trimers that redistribute and

464 cluster on the surface of virions following proteolytic Gag cleavage during maturation
465 (52). Considering the low number of Env trimers on natural HIV virions (53–55), this
466 clustering is crucial for establishing multiple receptor interactions necessary for virus
467 entry. To mimic the behavior of the virus, we prepared VLPs containing the X4 HIV-1
468 Env. HEK-293T cells were transiently transfected with pHXB2env, psPAX2, and, when
469 required, a pLentiGFP plasmid that encodes a GFP reporter gene flanked by LTR regions.
470 In this latter case, we generated LVPs because these budding particles contained genetic
471 material and could transduce target cells. Supernatants were collected 48-hours post
472 transfection, and VLPs were purified by ultracentrifugation and resuspended in PBS. The
473 structural integrity of the VLPs was confirmed using negative-stain electron microscopy
474 (Figure 2-Figure supplement 1A). Western blot analysis of the samples, culture media,
475 and clarified supernatants confirmed the presence of both gp120 and p24 in VLPs and
476 LVPs (Figure 2-Figure supplement 1B; Figure 2-Figure supplement 1-Source data 1). The
477 gp120-containing viral particles bound soluble CD4 (Figure 2-Figure supplement 1C) and
478 the corresponding LVPs successfully infected HEK-293CD4 cells, as demonstrated in
479 transduction assays (Figure 2-Figure supplement 1D, E). LVPs containing VSVG were
480 utilized as a positive control in these functional assays (Figure 2-figure supplement 1D,
481 E).

482 Immature HIV-1 particles exhibit reduced entry efficiency (56, 57). This effect
483 may stem from the rigidity of the immature Gag lattice beneath the viral membrane, which
484 hinders membrane fusion (58) interactions between Gag and Env glycoproteins, limiting
485 the lateral mobility of the sparsely distributed Env trimers and, consequently, impairing
486 the clustering necessary for efficient infection (13). Therefore, we evaluated the
487 maturation status of the generated VLPs using STED microscopy. We compared the
488 condensation of Gag and the distribution of Env molecules on the surface of the VLPs

489 with those observed on genetically immature particles and integrase-defective NL4-3ΔIN
490 virions, serving as controls (13). Env proteins were stained with the human mAb 2G12,
491 which specifically recognizes the gp120 domain. To avoid antibody-induced clustering,
492 we used purified Fab fragments of 2G12. The location of individual HIV-1 particles was
493 determined using the human mAb 37G12, which targets the Gag protein and served as a
494 "counterstain" reference (Figure 2A). By assessing Gag condensation, we estimated that
495 ~75% of the VLPs, both gp120-VLPs and Env(-) VLPs, were mature. These percentages
496 were lower for NL4-3ΔIN virions (~50%) and for immature VLPs (~16%) used as
497 controls (Figure 2B). Furthermore, we observed that 26.5% of the gp120-VLPs, 40.2%
498 of the NL4-3ΔIN virions, and 40.5% of the immature VLPs expressed gp120. As a
499 control, the anti-gp120 2G12 Fab did not stain particles lacking the Env (Env(-) VLPs)
500 (Figure 2A, C), confirming the specificity of the staining. Moreover, STED analysis
501 revealed differences in Env distribution between gp120-VLPs and NL4-3ΔIN virions, as
502 previously observed between mature and immature particles (13). Specifically, gp120
503 staining intensity was higher for NL4-3ΔIN particles than for gp120-VLPs (NL4-3ΔIN
504 1,786 a.u. vs. gp120-VLPs 1,223 a.u.) (Figure 2D), suggesting a lower expression of Env
505 proteins in the latter or a lower incorporation of the Env proteins into the VLPs. Analysis
506 of gp120 intensity per particle demonstrated that g120-VLPs had lower levels of
507 gp120/particle than NL4-3ΔIN virions (Figure 2E). These data confirmed the mature state
508 of the gp120-VLPs generated and indicated that they contained a reduced number of
509 gp120/particle, similar to or even lower than that found in primary HIV-1 viruses (55).

510 Next, we employed SPT-TIRF to investigate how gp120-VLPs affect CXCR4
511 dynamics in JKCD4^{+}X4^{-} cells that were transiently transfected with CXCR4-AcGFP
512 (Figure 3-videos 1-3). Analysis indicated that the gp120-VLPs significantly reduced
513 overall receptor diffusivity (basal, $D_{1\text{–}4}$ = 0.025 μm^2 s^{-1}; Env(-) VLPs, $D_{1\text{–}4}$ = 0.017 μm^2

514 s^{-1}; gp120-VLPs D_{1-4} = 0.012 $\mu m^2 s^{-1}$) (Figure 3A). In all the cases, most of the
515 trajectories corresponded to confined movement (Figure 3-Figure supplement 1) Under
516 these conditions, we found predominantly CXCR4 monomers and dimers at steady-state,
517 and their proportion decreased upon VLP treatment (basal ~99%; Env(-) VLPs ~91%;
518 gp120-VLPs ~71%). Consequently, the percentage of nanoclusters containing ≥3
519 receptors/particle increased (~1%, basal; ~9%, VLPs; ~29%, gp120-VLPs) (Figure 3B).
520 These findings were consistent with the MSI values (basal 761 a.u.; Env(-) VLPs 1,150
521 a.u.; gp120-VLPs 1,898 a.u.) (Figure 3C). Further investigations are needed to elucidate
522 the precise mechanism involved in the effect induced by the Env(-) VLPs on the dynamics
523 of the receptors.

524 Our results indicated that, similar to the effect triggered by soluble X4-gp120,
525 VLPs containing HIV-1 Env also triggered CXCR4 nanoclustering. To understand the
526 role of CXCR4 clustering in HIV-1 infection, we next analyzed the behavior of the
527 WHIM mutant CXCR4, $CXCR4^{R334X}$, which does not oligomerize in the presence of
528 CXCL12 (28). $CXCR4^{R334X}$ is a natural mutant of CXCR4 that binds CXCL12 (59–61),
529 but is not internalized in response to the ligand; in fact, it is a gain-of-function receptor
530 for this ligand (62). SPT-TIRF-M analysis of $JKCD4^+X4^-$ cells transiently transfected
531 with $CXCR4^{R334X}$-AcGFP (Figure 4-videos 1-3) demonstrated that, unlike the effect
532 described for CXCL12, the VLPs containing gp120 triggered $CXCR4^{R334X}$
533 oligomerization (basal MSI 669 a.u.; Env(-) VLPs MSI 909 a.u.; gp120-VLPs MSI 1,730
534 a.u.) (Figure 4A) and promoted a significant reduction in overall receptor diffusivity
535 (basal, median D_{1-4} = 0.021 $\mu m^2 s^{-1}$; gp120-VLPs, median D_{1-4} = 0.014 $\mu m^2 s^{-1}$) (Figure
536 4B) without significant differences in the percentage of trajectories with distinct type of
537 diffusion, again most of them exhibited confined movement (Figure 4-Figure supplement
538 1). Furthermore, gp120-VLP binding reduced the percentage of $CXCR4^{R334X}$ monomers

539 and dimers (steady-state ~99%; gp120-VLPs ~80%), while concurrently increasing the
540 percentage of nanoclusters containing ≥3 receptors/particle (basal ~1%; gp120-VLPs
541 ~20%) (Figure 4C).

542 All these data and other previously reported findings (28), indicate that CXCL12
543 triggers CXCR4 clustering at the cell membrane but does not induce $CXCR4^{R334X}$
544 oligomers. By contrast, gp120-VLPs binding stabilized CD4 complexes with both
545 CXCR4 and $CXCR4^{R334X}$ and promoted oligomerization of both co-receptors. It is thus
546 plausible that the conformation of CXCR4 and $CXCR4^{R334X}$ may differ between both
547 experimental conditions.

548 **CD4 expression alters the conformation adopted by CXCR4**

549 Our results support a model where CXCL12 binds to either CXCR4 or $CXCR4^{R334X}$ (28).
550 By contrast, X4-gp120, whether alone or within the viral context, associates these co-
551 receptors when they are complexed with CD4. It is known that CD4/CXCR4 complexes
552 might facilitate co-operative interactions with HIV-1 during viral adsorption and/or entry
553 into human leukocytes (63).

554 To confirm the interaction between CD4 and CXCR4 (22) and to assess whether
555 $CXCR4^{R334X}$ could also interact with CD4, we conducted FRET analyses. Our results
556 demonstrated positive FRET signals for both complexes: CD4/CXCR4 ($FRET_{50}$=2.71)
557 and CD4/$CXCR4^{R334X}$ ($FRET_{50}$=0.40) (Figure 5A, B). As a control, we observed minimal
558 residual energy transfer in cells co-transfected with CD4-CFP and $5HT_{2B}$-YFP (Figure
559 5C). The presence of CD4/CXCR4 and CD4/$CXCR4^{R334X}$ heterodimers was also
560 investigated *in silico* using alphaFold3 (64) (Figure 5-Figure supplement 1). We focused
561 on the interaction between the transmembrane and intracellular fragments of CD4 and
562 both CXCR4 and $CXCR4^{R334X}$. The predicted template modeling (pTM) scores for both
563 complexes were close to 0.7, suggesting a reliable prediction of these interactions. The

564 modeling also indicated a preferred association of CD4 with CXCR4 between
565 transmembrane helices IV and V, although further analysis is needed to precisely
566 determine the interaction site. These data align with previous reports demonstrating a
567 constitutive association between CD4 and CXCR4 that can influence HIV-1 infection
568 (22, 65–68) and our results extend this observation to the naturally occurring $CXCR4^{R334X}$
569 mutant. Furthermore, we observed increased FRET efficiency in both CD4-CXCR4 and
570 CD4-$CXCR4^{R334X}$ complexes upon gp120-VLPs binding (Figure 5D, E), confirming that
571 the VLPs induce conformational changes in these heterodimers.

572 Productive HIV-1 infection of $CD4^{+}$ cells markedly diminishes cell-surface
573 expression of CD4 (69, 70). However, the impact on chemokine receptors is less clear.
574 While some studies report a complete loss of CCR5 surface staining on cells chronically
575 infected with R5 viruses (71) the effect on CXCR4 varies (71, 72). Using flow cytometry,
576 we investigated how stimulation with X4-gp120 affects the cell-surface expression of
577 CD4, CXCR4, and $CXCR4^{R334X}$. Consistent with previous findings (73), CXCL12
578 induced rapid internalization of CXCR4 without altering $CXCR4^{R334X}$ levels at the cell
579 surface. By contrast, X4-gp120 caused a gradual, slight decrease in the surface expression
580 of both receptors. Furthermore, CXCL12 did not affect CD4 surface levels, whereas X4-
581 gp120 induced a gradual decline in CD4 expression (Figure 6A, B).

582 Taken together, our FRET and internalization experiments suggest that the effects
583 of X4-gp120 on CXCR4 and $CXCR4^{R334X}$ differ from those triggered by CXCL12 and
584 are dependent on their interaction with CD4.

585 Next, we investigated whether CD4/$CXCR4^{R334X}$ complexes could also support
586 primary HIV-1 infection. Flow cytometry analysis showed no significant difference in
587 the ability of Jurkat cells expressing either CXCR4 or $CXCR4^{R334X}$ to bind X4-gp120
588 (Figure 7A). In agreement, *in vitro* fusion assays using cells expressing CD4/CXCR4 or

589 CD4/CXCR4^{R334X}, and target cells expressing HIV pHXB2 Env, demonstrated a
590 significant increase in fusion events and syncytium formation in both Jurkat cell types
591 (Figure 7B, C). We then tested whether PBMCs isolated from a WHIM patient and
592 healthy donors were equally susceptible to infection by a primary X4 HIV-1_{NL4-3} viral
593 strain. We first analyzed the expression of CD4, and CXCR4 or CXCR4^{R334X} on these
594 PBMC samples by flow cytometry (Figure 7-Figure supplement 1). Subsequently, cells
595 were stimulated with PHA and IL-2, and 48 hours later, inoculated with a primary X4
596 HIV-1_{NL4-3} virus at a MOI of 0.001 for 120 minutes. ELISA measurements of p24 levels
597 in the culture medium at various time points revealed similar viral infection rates in both
598 Healthy and WHIM PBMCs (Figure 7D).

599 Collectively, these data indicate that T cells from a WHIM patient exhibit similar
600 infection and viral replication rates with those isolated from healthy donors. Furthermore,
601 these data suggest that HIV-1 might modulate the conformation adopted by CXCR4 at
602 the cell membrane, which is associated with HIV-1 infection. The CXCR4 conformation
603 stabilized by HIV-1 binding likely differs from that induced by CXCL12 binding and
604 therefore supports a direct effect of the interactions with CD4 in establishing a permissive
605 conformation of CXCR4 for HIV-1 infection.

606 **Discussion**

607 The process of HIV-1 infection begins with the binding of the trimeric HIV-1 Env
608 glycoprotein to the CD4 receptor on the target cell surface (74–76). Research indicates
609 that when the viral and cellular membranes are spatially distant, the HIV-1 Env trimers
610 initially engage only a single CD4 molecule, and as the Env moves closer to the
611 membrane and adopts an open conformation it gains the ability to bind a second and a
612 third CD4 molecule (24). CD4 binding thus induces critical conformational changes
613 within the gp120 subunit of Env that enable subsequent engagement of the co-receptors

614 CCR5 or CXCR4. Receptor and co-receptor engagement trigger further conformational
615 changes in the Env gp41 subunits, ultimately mediating the necessary fusion of the viral
616 and host cell membranes.

617 Competitive receptor inhibitors, such as soluble synthetic CD4 (sCD4), synthetic
618 CD4 peptides, and anti-CD4 binding site antibodies have been shown to effectively block
619 infection both *in vitro* (77, 78) and *in vivo* (79, 80). Notably, virus-like nanoparticles
620 displaying clustered membrane-associated CD4 demonstrated significantly greater
621 efficacy at blocking infection compared with sCD4, CD4-Ig, or the broadly neutralizing
622 monoclonal antibody 3BNC117 (81). These findings collectively suggest that the virus
623 may induce CD4 clustering to promote cell infection. Consistent with this idea, single-
624 molecule super-resolution imaging has revealed that CD4 molecules on the cell
625 membrane exist predominantly as individual molecules or small clusters (up to 4
626 molecules), and that the size and number of these clusters increase upon virus binding or
627 gp120 activation (19). These data therefore support a model where viral binding triggers
628 a nanoscale reorganization of CD4 on the plasma membrane, a process necessary for cell
629 infection. This observation aligns with substantial evidence indicating that various cell-
630 surface receptors are organized into clusters (23, 82). For instance, T-cell receptors on T
631 cells coalesce into nanoclusters within and around immune synapses prior to signal
632 transduction (83, 84). Receptor clustering has been also demonstrated for numerous other
633 transmembrane receptors, such as neurotransmitter receptors (85) and immune receptors
634 (86, 87). Furthermore, studies analyzing receptor dynamics during cell movement using
635 SPT have shown that chemokine-mediated receptor clustering is essential for cells to
636 accurately sense chemoattractant gradients (27, 28).

637 Here, using SPT-TIRF-M analysis on Jurkat cells, we found that both recombinant
638 X4-gp120 and VLPs displaying X4 HIV-1 Env (with fewer gp120 molecules) actively

639 promote CXCR4 clustering and modify its membrane dynamics in a CD4-dependent
640 manner. Our data show that, similar to the effect of CXCL12, gp120 binding to CXCR4
641 leads to a significant decrease in the number of monomers and dimers, while increasing
642 the proportion of larger, generally immobile nanoclusters. Previous studies utilizing
643 immunoelectron microscopy have suggested that CCR5, CXCR4, and CD4 are mainly
644 localized on microvilli and tend to form distinct, uniform microclusters in all cell types
645 examined (63). This clustering is thought to enhance co-operative interactions with HIV-
646 1 during virus adsorption and subsequent entry into human leukocytes (63). Single-
647 molecule force spectroscopy has also revealed that the force and duration required to
648 break apart the gp120/CCR5/CD4 complex are greater than those required for the
649 gp120/CD4 bond (88). The formation of CCR5/CD4/CXCR4 oligomers is implicated in
650 reducing the infectivity of X4 HIV-1 in cells that also express CCR5 (22).

651 The data suggest that exposure to HIV-1 triggers several rearrangements of cell
652 receptors, highlighting the significance of these changes in facilitating viral entry into
653 target cells. Receptor clustering, a process known to enhance cell sensitivity (89), also
654 promotes efficient cell signal transmission (90), and increases the robustness of signaling
655 systems (91). Indeed, it is well established that HIV-1 promotes CD4- and CXCR4-
656 mediated signaling events that facilitate viral entry and infection of host cells (39, 92–
657 95). We observed that gp120 triggered the phosphorylation of Lck, Akt, and ERK1/2, and
658 promoted cell polarization, although this latter effect was less pronounced than that
659 induced by CXCL12. Furthermore, in lipid bilayer assays using ICAM-1 as a substrate,
660 gp120 mediated Jurkat cell adhesion but did not significantly promote cell migration
661 compared with CXCL12. While soluble gp120 has been used to investigate certain HIV-
662 1 effects on cells (39, 43, 96), employing saturating concentrations of the glycoprotein
663 might lead to non-specific effects on the dynamics of receptors and co-receptors at the

664 cell membrane. Moreover, the conformation of recombinant gp120 may not accurately
665 reflect its physiological structure on intact HIV-1 particles. Within virions, the Env
666 glycoprotein forms heterotrimeric gp120 non-covalently associated with three gp41
667 molecules. To address these limitations, we generated VLPs displaying the X4 HIV-1
668 Env. Super-resolution microscopy confirmed the maturity of the gp120-VLPs, expressing
669 a very low number of gp120 trimers on their surface, even fewer than the 7 to 14 Env
670 trimers per virus particle previously reported on primary isolated virions (54, 97, 98)
671 Similar to soluble recombinant gp120, these VLPs also induced CXCR4 clustering and
672 altered receptor dynamics. These findings thus confirm that the effects observed with X4-
673 gp120 are not artifacts resulting from the conformation of the soluble gp120 or to the use
674 of saturating concentrations. Receptor clustering was initiated through binding of gp120-
675 VLPs to CD4 and CXCR4, as neither X4-gp120 nor the VLPs associated with CXCR4 in
676 the absence of CD4. We confirmed this using a mutant CXCR4, $CXCR4^{R334X}$, which does
677 not oligomerize in the presence of CXCL12 (28). $CXCR4^{R334X}$ is found in cells of patients
678 with WHIM syndrome, a rare combined immunodeficiency characterized by the presence
679 of warts, hypogammaglobulinemia, recurrent bacterial infections and myelokathexis
680 symptoms (29). In these patients, the inability of CXCL12 to induce receptor
681 oligomerization leads to defects in actin dynamics, preventing proper sensing of
682 chemoattractant gradients (28, 99). We investigated how VLPs containing the X4 HIV-1
683 Env affected the dynamics of $CXCR4^{R334X}$ in cells expressing CD4. Surprisingly, the X4
684 HIV-1 Env caused a significant reduction in $CXCR4^{R334X}$ monomers and dimers, while
685 increasing the proportion of larger nanoclusters, which were generally immobile. These
686 findings suggest that CXCL12 and gp120 VLPs have different effects on chemokine
687 receptor dynamics, leading us to hypothesize that the structure of CXCR4, whether or not
688 it is associated with CD4, could explain these observations. AlphaFold predictions and

689 FRET analysis confirmed the formation of CD4/CXCR4 complexes (22) and supported
690 the existence of CD4/CXCR4^{R334X} heterodimers. In both cases, gp120-VLPs binding
691 altered the conformations. These findings correlate with the syncytia formation observed
692 in *in vitro* fusion experiments between cells expressing the X4 HIV-1 Env and target cells
693 expressing either CD4/CXCR4 or CD4/CXCR4^{R334X}, and with the infection of PBMCs
694 from both WHIM patients and healthy donors when incubated with primary X4-HIV-1.
695 These findings also indicate that WHIM mutations do not protect against HIV-1 infection,
696 consistent with a previous *in vitro* study showing that CD4^{+}U87 cells expressing
697 CXCR4^{R334X} or CXCR4 are equally susceptible to a luciferase-expressing pseudotyped
698 virus infection (60). To better reflect natural infection kinetics, we employed fully
699 replication-competent viruses rather than pseudotyped systems. Furthermore, we
700 monitored viral dynamics over a seven-day period, providing a longitudinal perspective
701 that extends beyond the limitations of a standard 24-hour snapshot. Beyond inducing
702 CXCR4 aggregation, we observed that X4-gp120 promoted the internalization of CD4
703 and CXCR4 and, surprisingly, also triggered the internalization of CXCR4^{R334X}. This
704 mutant receptor cannot internalize in response to CXCL12 because it lacks the last 19 C-
705 terminal amino acids, which are necessary for GRK-mediated Ser/Thr phosphorylation
706 and β-arrestin recruitment (29, 100). Some studies suggest that HIV-1 glycoproteins can
707 reduce CD4 and CXCR4 levels during HIV-1 entry (72, 101, 102), proposing receptor-
708 mediated endocytosis as an alternative HIV-1 entry mechanism (103–108). Other reports
709 even indicate a ligand-mediated co-endocytosis of CD4 and the chemokine receptors
710 during HIV-1 entry (109–111). HIV-1-mediated endocytosis might also explain the
711 reduction of CD4 and CXCR4^{R334X} at the cell membrane and the similar infection rates
712 in PBMCs from WHIM patients and healthy donors. Although direct evidence for the
713 internalization of CD4 and CXCR4 as complexes is lacking, their co-localization in lipid

714 rafts during HIV-1 infection (32, 112, 113) and their ability to form heterocomplexes (22)
715 strongly suggest they could be endocytosed together. Therefore, we hypothesize that
716 gp120 binding to CD4 stabilizes CD4/CXCR4 complexes, and that the conformation of
717 CXCR4 within these complexes might differ from that of CXCR4 homodimers.

718 We also detected a residual but significant effect of Env(-) VLPs on the dynamics
719 of both CXCR4 and of CXCR4^{R334X}. This is likely not receptor-mediated, as these control
720 VLPs lacked the X4 HIV-1 Env. While further experiments are needed, a potential
721 interaction between the lipids and or cell adhesion molecules derived from the cells where
722 the virions were produced, and those in the cell membrane could explain this observation.
723 It is well established that the lipid composition of the cell membrane influences ligand-
724 mediated chemokine receptor oligomerization and dynamics (114, 115). Additionally,
725 glycosaminoglycans, such as heparin and heparan sulphate, might play a role in the
726 attachment of virions to various cell types (116–118). Although their effects on R5 strains
727 are debated (119–121), the concentrations of these glycosaminoglycans vary considerably
728 between cells (122). Besides, some viruses bind lectins at the cell membrane, for instance
729 some microdomains of C-type lectin DC-SIGN have been described as portals for HIV-
730 1 entry (123, 124).

731 Our data indicate that HIV-1 not only affects CD4 dynamics, which is well known,
732 but also alters the spatial distribution and dynamics of CXCR4 in a manner distinct from
733 the effects of its natural ligand, CXCL12. While HIV-1 binding involves CD4/CXCR4
734 complexes, CXCL12 binds exclusively to CXCR4, potentially leading to different effects
735 on CXCR4 conformations. These findings might also explain why HIV-1 induced the
736 endocytosis of both CD4/CXCR4 and CD4/CXCR4^{R334X} complexes, whereas CXCL12
737 did not mediate the internalization of either CD4 or the CD4/CXCR4^{R334X} complex. This
738 suggests that the interaction of both co-receptors with CD4 may result in different

739 conformations of CXCR4 and CXCR4^{R334X} compared with their respective homodimers.
740 The interaction motif between CD4 and CXCR4 should be considered a crucial target for
741 disrupting complex dynamics at the cell membrane, potentially opening new avenues for
742 anti-HIV-1 therapies.

743 **Acknowledgements**
744

745 This work was supported by grants from the Spanish Ministry of Science and Innovation
746 (PID2020-114980RB-I00 and PID2023-146301OB-I00) to MM and (PID2022-
747 140651NB-I00) to CS, and (PID2022-139271OB-I00 and CB21/13/00063) to JM-P. EG-
748 C and BS were supported by the program Apoyos Centros de Excelencia S.O. of the
749 Spanish Ministry of Science and Innovation (SEV-2017-0712). AQ-F and SRG ere
750 included in the doctoral program of the Department of Molecular Biosciences and of
751 Biology, respectively, Universidad Autónoma de Madrid, and are supported by the Fondo
752 de Personal Investigador (FPI) program of the Spanish Ministry for Science and
753 Innovation (PRE2018-083201 and PRE2019-087966, respectively). EAB is included in
754 the doctoral program of Biomedicine, University of Barcelona, and is supported by the
755 FPI program of the Spanish Ministry for Science and Innovation (PRE2022-000847). RA-
756 B is supported by the Garantía Juvenil program of the Regional Government of Madrid,
757 Spain (CAM20_CNB_AI_07). LIGG receives funding from Institute of Health, Carlos
758 III co-funded by Fondos FEDER Project FIS PI21/01642. We also acknowledge the
759 technical help of the Advance Light Microscopy Unit at the CNB/CSIC.
760

761 JMP has received research funding, consultancy fees, and lecture sponsorships from and
762 has served on advisory boards for various companies (AbiVax, AstraZeneca, MSD,
763 Gilead Sciences, ViiV Healthcare, Johnson & Johnson) outside the scope of this article.
764 The rest of the authors declare no competing interests.

765

766 **Bibliography**

767 1. M. Kowalski, *et al.*, Functional regions of the envelope glycoprotein of human
768 immunodeficiency virus type 1. *Science* **237**, 1351–1355 (1987).
769 2. M. Lu, S. C. Blacklow, P. S. Kim, A trimeric structural domain of the HIV-1
770 transmembrane glycoprotein. *Nature Structural Biology 1995 2:12* **2**, 1075–1082
771 (1995).
772 3. H. Choe, *et al.*, The beta-chemokine receptors CCR3 and CCR5 facilitate
773 infection by primary HIV-1 isolates. *Cell* **85**, 1135–1148 (1996).
774 4. Y. Feng, C. C. Broder, P. E. Kennedy, E. A. Berger, HIV-1 entry cofactor:
775 functional cDNA cloning of a seven-transmembrane, G protein-coupled receptor.
776 *Science* **272**, 872–877 (1996).
777 5. S. M. Wolinsky, *et al.*, Adaptive evolution of human immunodeficiency virus-
778 type 1 during the natural course of infection. *Science* **272**, 537–542 (1996).
779 6. Z. H. Lu, *et al.*, Evolution of HIV-1 coreceptor usage through interactions with
780 distinct CCR5 and CXCR4 domains. *Proc. Natl. Acad. Sci. U. S. A.* **94**, 6426–
781 6431 (1997).
782 7. R. I. Connor, H. Mohri, Y. Cao, D. D. Ho, Increased viral burden and
783 cytopathicity correlate temporally with CD4+ T-lymphocyte decline and clinical
784 progression in human immunodeficiency virus type 1-infected individuals. *J.*
785 *Virol.* **67**, 1772–1777 (1993).
786 8. C. C. Carter, *et al.*, HIV-1 Utilizes the CXCR4 Chemokine Receptor to Infect
787 Multipotent Hematopoietic Stem and Progenitor Cells. *Cell Host Microbe* **9**,
788 223–234 (2011).
789 9. N. R. Landau, M. Warton, D. R. Littman, The envelope glycoprotein of the
790 human immunodeficiency virus binds to the immunoglobulin-like domain of
791 CD4. *Nature* **334**, 159–162 (1988).
792 10. J. Arthos, *et al.*, Identification of the residues in human CD4 critical for the
793 binding of HIV. *Cell* **57**, 469–481 (1989).
794 11. W. Zhang, *et al.*, Conformational changes of gp120 in epitopes near the CCR5
795 binding site are induced by CD4 and a CD4 miniprotein mimetic. *Biochemistry*
796 **38**, 9405–9416 (1999).
797 12. R. W. Doms, J. P. Moore, HIV-1 membrane fusion: targets of opportunity. *J. Cell*
798 *Biol.* **151** (2000).
799 13. J. Chojnacki, *et al.*, Maturation-dependent HIV-1 surface protein redistribution
800 revealed by fluorescence nanoscopy. *Science* **338**, 524–528 (2012).
801 14. V. Buzon, *et al.*, Crystal structure of HIV-1 gp41 including both fusion peptide
802 and membrane proximal external regions. *PLoS Pathog.* **6**, 1–7 (2010).
803 15. M. Pancera, *et al.*, Structure of HIV-1 gp120 with gp41-interactive region reveals
804 layered envelope architecture and basis of conformational mobility. *Proc. Natl.*
805 *Acad. Sci. U. S. A.* **107**, 1166–1171 (2010).
806 16. H. Garg, M. Viard, A. Jacobs, R. Blumenthal, Targeting HIV-1 gp41-induced
807 fusion and pathogenesis for anti-viral therapy. *Curr. Top. Med. Chem.* **11**, 2947–
808 2958 (2011).
809 17. M. Barrero-Villar, *et al.*, Moesin is required for HIV-1-induced CD4-CXCR4
810 interaction, F-actin redistribution, membrane fusion and viral infection in
811 lymphocytes. *J. Cell Sci.* **122**, 103–113 (2009).
812 18. S. Jiménez-Baranda, *et al.*, Filamin-A regulates actin-dependent clustering of
813 HIV receptors. *Nat. Cell Biol.* **9**, 838–846 (2007).

814 19. Y. Yuan, *et al.*, Single-Molecule Super-Resolution Imaging of T-Cell Plasma
815 Membrane CD4 Redistribution upon HIV-1 Binding. *Viruses* **13** (2021).
816 20. C. K. Lapham, *et al.*, Evidence for cell-surface association between fusin and the
817 CD4-gp120 complex in human cell lines. *Science* **274**, 602–605 (1996).
818 21. S. Ugolini,', *et al.*, HIV-1 gp120 Induces an Association Between CD4 and the
819 Chemokine Receptor CXCR4'. *The Journal of Immunology* **159**, 3000–3008
820 (1997).
821 22. L. Martínez-Muñoz, *et al.*, CCR5/CD4/CXCR4 oligomerization prevents HIV-1
822 gp120IIIB binding to the cell surface. *Proc. Natl. Acad. Sci. U. S. A.* **111** (2014).
823 23. N. C. Hartman, J. T. Groves, Signaling clusters in the cell membrane. *Curr.*
824 *Opin. Cell Biol.* **23**, 370–376 (2011).
825 24. W. Li, *et al.*, HIV-1 Env trimers asymmetrically engage CD4 receptors in
826 membranes. *Nature* **623**, 1026–1033 (2023).
827 25. M. F. Krummel, M. D. Sjaastad, C. W. Wulfing, M. M. Davis, Differential
828 clustering of CD4 and CD3zeta during T cell recognition. *Science* **289**, 1349–
829 1352 (2000).
830 26. H. Kao, J. Lin, D. R. Littman, A. S. Shaw, P. M. Allen, Regulated movement of
831 CD4 in and out of the immunological synapse. *J. Immunol.* **181**, 8248–8257
832 (2008).
833 27. L. Martínez-Muñoz, *et al.*, Separating Actin-Dependent Chemokine Receptor
834 Nanoclustering from Dimerization Indicates a Role for Clustering in CXCR4
835 Signaling and Function. *Mol. Cell* **70**, 106-119.e10 (2018).
836 28. E. M. García-Cuesta, *et al.*, Altered CXCR4 dynamics at the cell membrane
837 impairs directed cell migration in WHIM syndrome patients. *Proc. Natl. Acad.*
838 *Sci. U. S. A.* **119** (2022).
839 29. Q. Liu, *et al.*, WHIM syndrome caused by a single amino acid substitution in the
840 carboxy-tail of chemokine receptor CXCR4. *Blood* **120**, 181–189 (2012).
841 30. E. M. García-Cuesta, *et al.*, Altered CXCR4 dynamics at the cell membrane
842 impairs directed cell migration in WHIM syndrome patients. *Proc. Natl. Acad.*
843 *Sci. U. S. A.* **119** (2022).
844 31. S. R. Gardeta, *et al.*, Sphingomyelin Depletion Inhibits CXCR4 Dynamics and
845 CXCL12-Mediated Directed Cell Migration in Human T Cells. *Front. Immunol.*
846 **13** (2022).
847 32. S. Mañes, *et al.*, Membrane raft microdomains mediate lateral assemblies
848 required for HIV-1 infection. *EMBO Rep.* **1**, 190–196 (2000).
849 33. L. Martínez-Muñoz, *et al.*, Separating Actin-Dependent Chemokine Receptor
850 Nanoclustering from Dimerization Indicates a Role for Clustering in CXCR4
851 Signaling and Function. *Mol. Cell* **70**, 106-119.e10 (2018).
852 34. G. Del Real, *et al.*, Blocking of HIV-1 infection by targeting CD4 to nonraft
853 membrane domains. *J. Exp. Med.* **196**, 293–301 (2002).
854 35. Y. R. Carrasco, S. J. Fleire, T. Cameron, M. L. Dustin, F. D. Batista, LFA-
855 1/ICAM-1 interaction lowers the threshold of B cell activation by facilitating B
856 cell adhesion and synapse formation. *Immunity* **20**, 589–599 (2004).
857 36. L. Martínez Muñoz, *et al.*, Dynamic regulation of CXCR1 and CXCR2 homo-
858 and heterodimers. *J. Immunol.* **183**, 7337–7346 (2009).
859 37. K. Jaqaman, *et al.*, Robust single-particle tracking in live-cell time-lapse
860 sequences. *Nat. Methods* **5**, 695–702 (2008).
861 38. S. Dorsch, K. N. Klotz, S. Engelhardt, M. J. Lohse, M. Bünemann, Analysis of
862 receptor oligomerization by FRAP microscopy. *Nat. Methods* **6**, 225–230 (2009).

863 39. K. Balabanian, *et al.*, CXCR4-Tropic HIV-1 Envelope Glycoprotein Functions as
864 a Viral Chemokine in Unstimulated Primary CD4 + T Lymphocyteskk. *The*
865 *Journal of Immunology* **173**, 7150–7160 (2004).
866 40. J. Arthos, *et al.*, CCR5 signal transduction in macrophages by human
867 immunodeficiency virus and simian immunodeficiency virus envelopes. *J. Virol.*
868 **74**, 6418–6424 (2000).
869 41. G. Briand, B. Barbeau, M. Tremblay, Binding of HIV-1 to its receptor induces
870 tyrosine phosphorylation of several CD4-associated proteins, including the
871 phosphatidylinositol 3-kinase. *Virology* **228**, 171–179 (1997).
872 42. A. P. Curnock, M. K. Logan, S. G. Ward, Chemokine signalling: pivoting around
873 multiple phosphoinositide 3-kinases. *Immunology* **105**, 125–136 (2002).
874 43. A. Yoder, *et al.*, HIV Envelope-CXCR4 Signaling Activates Cofilin to Overcome
875 Cortical Actin Restriction in Resting CD4 T Cells. *Cell* **134**, 782–792 (2008).
876 44. S. Iyengar, J. E. K. Hildreth, D. H. Schwartz, Actin-dependent receptor
877 colocalization required for human immunodeficiency virus entry into host cells.
878 *J. Virol.* **72**, 5251–5255 (1998).
879 45. A. G. Bukrinskaya, HIV-1 assembly and maturation. *Arch. Virol.* **149**, 1067–
880 1082 (2004).
881 46. S. J. Plowman, C. Muncke, R. G. Parton, J. F. Hancock, H-ras, K-ras, and inner
882 plasma membrane raft proteins operate in nanoclusters with differential
883 dependence on the actin cytoskeleton. *Proc. Natl. Acad. Sci. U. S. A.* **102**, 15500–
884 15505 (2005).
885 47. J. A. Torreno-Pina, *et al.*, The actin cytoskeleton modulates the activation of
886 iNKT cells by segregating CD1d nanoclusters on antigen-presenting cells. *Proc.*
887 *Natl. Acad. Sci. U. S. A.* **113**, E772–E781 (2016).
888 48. P. M. Pereira, *et al.*, Fix Your Membrane Receptor Imaging: Actin Cytoskeleton
889 and CD4 Membrane Organization Disruption by Chemical Fixation. *Front.*
890 *Immunol.* **10** (2019).
891 49. C. Manzo, M. F. Garcia-Parajo, A review of progress in single particle tracking:
892 From methods to biophysical insights. *Reports on Progress in Physics* [Preprint]
893 (2015). Available at: http://www.ncbi.nlm.nih.gov/pubmed/26511974 [Accessed
894 11 January 2022].
895 50. H. Ewers, *et al.*, Single-particle tracking of murine polyoma virus-like particles
896 on live cells and artificial membranes. *Proc. Natl. Acad. Sci. U. S. A.* **102**,
897 15110–15115 (2005).
898 51. D. Calebiro, *et al.*, Single-molecule analysis of fluorescently labeled G-protein-
899 coupled receptors reveals complexes with distinct dynamics and organization.
900 *Proc. Natl. Acad. Sci. U. S. A.* **110**, 743–748 (2013).
901 52. J. Chojnacki, *et al.*, Envelope glycoprotein mobility on HIV-1 particles depends
902 on the virus maturation state. *Nat. Commun.* **8** (2017).
903 53. T. K. Hart, A. M. Klinkner, J. Ventre, P. J. Bugelski, Morphometric analysis of
904 envelope glycoprotein gp120 distribution on HIV-1 virions. *J. Histochem.*
905 *Cytochem.* **41**, 265–271 (1993).
906 54. P. Zhu, *et al.*, Electron tomography analysis of envelope glycoprotein trimers on
907 HIV and simian immunodeficiency virus virions. *Proc. Natl. Acad. Sci. U. S. A.*
908 **100**, 15812–15817 (2003).
909 55. P. Zhu, *et al.*, Distribution and three-dimensional structure of AIDS virus
910 envelope spikes. *Nature* **441**, 847–852 (2006).

911 56. T. Murakami, S. Ablan, E. O. Freed, Y. Tanaka, Regulation of human
912 immunodeficiency virus type 1 Env-mediated membrane fusion by viral protease
913 activity. *J. Virol.* **78**, 1026–1031 (2004).
914 57. D. J. Wyma, *et al.*, Coupling of human immunodeficiency virus type 1 fusion to
915 virion maturation: a novel role of the gp41 cytoplasmic tail. *J. Virol.* **78**, 3429–
916 3435 (2004).
917 58. N. R. Rauh, A. Schmidt, J. Bormann, E. A. Nigg, T. U. Mayer, Calcium triggers
918 exit from meiosis II by targeting the APC/C inhibitor XErp1 for degradation.
919 *Nature* **437**, 1048–1052 (2005).
920 59. K. Balabanian, *et al.*, WHIM syndromes with different genetic anomalies are
921 accounted for by impaired CXCR4 desensitization to CXCL12. *Blood* **105**,
922 2449–2457 (2005).
923 60. P. A. Hernandez, *et al.*, Mutations in the chemokine receptor gene CXCR4 are
924 associated with WHIM syndrome, a combined immunodeficiency disease. *Nat.*
925 *Genet.* **34**, 70–74 (2003).
926 61. J. M. Busillo, J. L. Benovic, Regulation of CXCR4 signaling. *Biochim. Biophys.*
927 *Acta* **1768**, 952–963 (2007).
928 62. D. H. Mcdermott, *et al.*, AMD3100 is a potent antagonist at CXCR4(R334X) , a
929 hyperfunctional mutant chemokine receptor and cause of WHIM syndrome. *J.*
930 *Cell. Mol. Med.* **15**, 2071–2081 (2011).
931 63. I. I. Singer, *et al.*, CCR5, CXCR4, and CD4 are clustered and closely apposed on
932 microvilli of human macrophages and T cells. *J. Virol.* **75**, 3779–3790 (2001).
933 64. J. Abramson, *et al.*, Accurate structure prediction of biomolecular interactions
934 with AlphaFold 3. *Nature* **630**, 493–500 (2024).
935 65. S. Basmaciogullari, B. Pacheco, S. Bour, J. Sodroski, Specific interaction of
936 CXCR4 with CD4 and CD8alpha: functional analysis of the CD4/CXCR4
937 interaction in the context of HIV-1 envelope glycoprotein-mediated membrane
938 fusion. *Virology* **353**, 52–67 (2006).
939 66. M. Zaitseva, *et al.*, Increased CXCR4-dependent HIV-1 fusion in activated T
940 cells: role of CD4/CXCR4 association. *J. Leukoc. Biol.* **78**, 1306–1317 (2005).
941 67. C. K. Lapham, M. B. Zaitseva, S. Lee, T. Romanstseva, H. Golding, Fusion of
942 monocytes and macrophages with HIV-1 correlates with biochemical properties
943 of CXCR4 and CCR5. *Nat. Med.* **5**, 303–308 (1999).
944 68. S. Lee, *et al.*, Coreceptor competition for association with CD4 may change the
945 susceptibility of human cells to infection with T-tropic and macrophagetropic
946 isolates of human immunodeficiency virus type 1. *J. Virol.* **74**, 5016–5023
947 (2000).
948 69. J. A. Hoxie, *et al.*, Alterations in T4 (CD4) protein and mRNA synthesis in cells
949 infected with HIV. *Science* **234**, 1123–1127 (1986).
950 70. M. J. Potash, D. J. Volsky, Viral Interference in HIV-1 Infected Cells. *Reviews in*
951 *Medical Virology Rev. Med. Virol* **8**, 203–211 (1998).
952 71. A. L. Chenine, Q. Sattentau, M. Moulard, Selective HIV-1-induced
953 downmodulation of CD4 and coreceptors. *Arch. Virol.* **145**, 455–471 (2000).
954 72. B. Choi, *et al.*, Down-regulation of cell surface CXCR4 by HIV-1. *Virol. J.* **5**
955 (2008).
956 73. K. Balabanian, B. Lagane, J. Pablos, L. L.- Blood, undefined 2005, WHIM
957 syndromes with different genetic anomalies are accounted for by impaired
958 CXCR4 desensitization to CXCL12. *ashpublications.orgK Balabanian, B*
959 *Lagane, JL Pablos, L Laurent, T Planchenault, O Verola, C Lebbe, D*
960 *KerobBlood, 2005•ashpublications.org*.

961 74. R. Wyatt, J. Sodroski, The HIV-1 envelope glycoproteins: fusogens, antigens,
962 and immunogens. *Science* **280**, 1884–1888 (1998).
963 75. R. Blumenthal, S. Durell, M. Viard, HIV entry and envelope glycoprotein-
964 mediated fusion. *J. Biol. Chem.* **287**, 40841–40849 (2012).
965 76. B. Chen, Molecular Mechanism of HIV-1 Entry. *Trends Microbiol.* **27**, 878–891
966 (2019).
967 77. A. Traunecker, J. Schneider, H. Kiefer, K. Karjalainen, Highly efficient
968 neutralization of HIV with recombinant CD4-immunoglobulin molecules. *Nature*
969 **339**, 68–70 (1989).
970 78. P. L. Nara, K. M. Hwang, D. M. Rausch, J. D. Lifson, L. E. Eiden, CD4 antigen-
971 based antireceptor peptides inhibit infectivity of human immunodeficiency virus
972 in vitro at multiple stages of the viral life cycle. *Proc. Natl. Acad. Sci. U. S. A.*
973 **86**, 7139–7143 (1989).
974 79. R. T. Schooley, *et al.*, Recombinant soluble CD4 therapy in patients with the
975 acquired immunodeficiency syndrome (AIDS) and AIDS-related complex. A
976 phase I-II escalating dosage trial. *Ann. Intern. Med.* **112**, 247–253 (1990).
977 80. J. O. Kahn, *et al.*, The safety and pharmacokinetics of recombinant soluble CD4
978 (rCD4) in subjects with the acquired immunodeficiency syndrome (AIDS) and
979 AIDS-related complex. A phase 1 study. *Ann. Intern. Med.* **112**, 254–261 (1990).
980 81. M. A. G. Hoffmann, *et al.*, Nanoparticles presenting clusters of CD4 expose a
981 universal vulnerability of HIV-1 by mimicking target cells. *Proc. Natl. Acad. Sci.*
982 *U. S. A.* **117**, 18719–18728 (2020).
983 82. W. W. A. Schamel, B. Alarcón, Organization of the resting TCR in nanoscale
984 oligomers. *Immunol. Rev.* **251**, 13–20 (2013).
985 83. Y. Razvag, *et al.*, T Cell Activation through Isolated Tight Contacts. *Cell Rep.*
986 **29**, 3506-3521.e6 (2019).
987 84. B. F. Lillemeier, *et al.*, TCR and Lat are expressed on separate protein islands on
988 T cell membranes and concatenate during activation. *Nat. Immunol.* **11**, 90–96
989 (2010).
990 85. P. Verstreken, H. J. Bellen, Meaningless minis? Mechanisms of neurotransmitter-
991 receptor clustering. *Trends Neurosci.* **25**, 383–385 (2002).
992 86. R. N. Germain, T-cell signaling: the importance of receptor clustering. *Curr.*
993 *Biol.* **7** (1997).
994 87. C. W. Cairo, Signaling by committee: receptor clusters determine pathways of
995 cellular activation. *ACS Chem. Biol.* **2**, 652–655 (2007).
996 88. M. I. Chang, P. Panorchan, T. M. Dobrowsky, Y. Tseng, D. Wirtz, Single-
997 molecule analysis of human immunodeficiency virus type 1 gp120-receptor
998 interactions in living cells. *J. Virol.* **79**, 14748–14755 (2005).
999 89. D. Bray, Protein molecules as computational elements in living cells. *Nature* **376**,
1000 307–312 (1995).
1001 90. W. Cho, R. V. Stahelin, Membrane-protein interactions in cell signaling and
1002 membrane trafficking. *Annu. Rev. Biophys. Biomol. Struct.* **34**, 119–151 (2005).
1003 91. T. Gurry, O. Kahramanoğullari, R. G. Endres, Biophysical mechanism for ras-
1004 nanocluster formation and signaling in plasma membrane. *PLoS One* **4** (2009).
1005 92. W. Popik, J. E. Hesselgesser, P. M. Pitha, Binding of human immunodeficiency
1006 virus type 1 to CD4 and CXCR4 receptors differentially regulates expression of
1007 inflammatory genes and activates the MEK/ERK signaling pathway. *J. Virol.* **72**,
1008 6406–6413 (1998).
1009 93. C. B. Davis, *et al.*, Signal transduction due to HIV-1 envelope interactions with
1010 chemokine receptors CXCR4 or CCR5. *J. Exp. Med.* **186**, 1793–1798 (1997).

1011 94. S. Pasquereau, G. Herbein, CounterAKTing HIV: Toward a "Block and Clear"
1012 Strategy? *Front. Cell. Infect. Microbiol.* **12** (2022).
1013 95. F. François, M. E. Klotman, Phosphatidylinositol 3-kinase regulates human
1014 immunodeficiency virus type 1 replication following viral entry in primary CD4+
1015 T lymphocytes and macrophages. *J. Virol.* **77**, 2539–2549 (2003).
1016 96. J. Deng, *et al.*, HIV Envelope gp120 Alters T Cell Receptor Mobilization in the
1017 Immunological Synapse of Uninfected CD4 T Cells and Augments T Cell
1018 Activation. *J. Virol.* **90**, 10513–10526 (2016).
1019 97. E. Chertova, *et al.*, Envelope glycoprotein incorporation, not shedding of surface
1020 envelope glycoprotein (gp120/SU), Is the primary determinant of SU content of
1021 purified human immunodeficiency virus type 1 and simian immunodeficiency
1022 virus. *J. Virol.* **76**, 5315–5325 (2002).
1023 98. M. C. DeSantis, J. H. Kim, H. Song, P. J. Klasse, W. Cheng, Quantitative
1024 Correlation between Infectivity and Gp120 Density on HIV-1 Virions Revealed
1025 by Optical Trapping Virometry. *J. Biol. Chem.* **291**, 13088–13097 (2016).
1026 99. E. M. García-Cuesta, *et al.*, Allosteric modulation of the CXCR4:CXCL12 axis
1027 by targeting receptor nanoclustering via the TMV-TMVI domain. *Elife* **13**
1028 (2024).
1029 100. R. Kumar, *et al.*, Reduced G protein signaling despite impaired internalization
1030 and β-arrestin recruitment in patients carrying a CXCR4Leu317fsX3 mutation
1031 causing WHIM syndrome. *JCI Insight* **8** (2023).
1032 101. R. Geleziunas, S. Bour, M. A. Wainberg, Cell surface down-modulation of CD4
1033 after infection by HIV-1. *FASEB J.* **8**, 593–600 (1994).
1034 102. P. Hubert, G. Bismuth, M. Körner, P. Debré, HIV-1 glycoprotein gp120 disrupts
1035 CD4-p56lck/CD3-T cell receptor interactions and inhibits CD3 signaling. *Eur. J.*
1036 *Immunol.* **25**, 1417–1425 (1995).
1037 103. J. Daecke, O. T. Fackler, M. T. Dittmar, H.-G. Kräusslich, Involvement of
1038 clathrin-mediated endocytosis in human immunodeficiency virus type 1 entry. *J.*
1039 *Virol.* **79**, 1581–1594 (2005).
1040 104. A. Aggarwal, *et al.*, HIV infection is influenced by dynamin at 3 independent
1041 points in the viral life cycle. *Traffic* **18**, 392–410 (2017).
1042 105. M. de la Vega, *et al.*, Inhibition of HIV-1 endocytosis allows lipid mixing at the
1043 plasma membrane, but not complete fusion. *Retrovirology* **8**, 99 (2011).
1044 106. K. Miyauchi, Y. Kim, O. Latinovic, V. Morozov, G. B. Melikyan, HIV enters
1045 cells via endocytosis and dynamin-dependent fusion with endosomes. *Cell* **137**,
1046 433–444 (2009).
1047 107. G. C. Carter, L. Bernstone, D. Baskaran, W. James, HIV-1 infects macrophages
1048 by exploiting an endocytic route dependent on dynamin, Rac1 and Pak1.
1049 *Virology* **409**, 234–250 (2011).
1050 108. B. Van Wilgenburg, M. D. Moore, W. S. James, S. A. Cowley, The productive
1051 entry pathway of HIV-1 in macrophages is dependent on endocytosis through
1052 lipid rafts containing CD4. *PLoS One* **9** (2014).
1053 109. M. Toyoda, *et al.*, Differential Ability of Primary HIV-1 Nef Isolates To
1054 Downregulate HIV-1 Entry Receptors. *J. Virol.* **89**, 9639–9652 (2015).
1055 110. S. Venzke, N. Michel, I. Allespach, O. T. Fackler, O. T. Keppler, Expression of
1056 Nef downregulates CXCR4, the major coreceptor of human immunodeficiency
1057 virus, from the surfaces of target cells and thereby enhances resistance to
1058 superinfection. *J. Virol.* **80**, 11141–11152 (2006).

1059 111. L.-A. Gobeil, R. Lodge, M. J. Tremblay, Macropinocytosis-like HIV-1
1060 internalization in macrophages is CCR5 dependent and leads to efficient but
1061 delayed degradation in endosomal compartments. *J. Virol.* **87**, 735–745 (2013).
1062 112. W. Popik, T. M. Alce, W.-C. Au, Human immunodeficiency virus type 1 uses
1063 lipid raft-colocalized CD4 and chemokine receptors for productive entry into
1064 CD4(+) T cells. *J. Virol.* **76**, 4709–4722 (2002).
1065 113. N. F. Neel, E. Schutyser, J. Sai, G. H. Fan, A. Richmond, Chemokine receptor
1066 internalization and intracellular trafficking. *Cytokine Growth Factor Rev.* **16**,
1067 637–658 (2005).
1068 114. S. R. Gardeta, *et al.*, Sphingomyelin Depletion Inhibits CXCR4 Dynamics and
1069 CXCL12-Mediated Directed Cell Migration in Human T Cells. *Front. Immunol.*
1070 **13** (2022).
1071 115. M. A. Hauser, *et al.*, Inflammation-Induced CCR7 Oligomers Form Scaffolds to
1072 Integrate Distinct Signaling Pathways for Efficient Cell Migration. *Immunity* **44**,
1073 59–72 (2016).
1074 116. H. A. Harrop, C. C. Rider, Heparin and its derivatives bind to HIV-1 recombinant
1075 envelope glycoproteins, rather than to recombinant HIV-1 receptor, CD4.
1076 *Glycobiology* **8**, 131–137 (1998).
1077 117. I. Mondor, S. Ugolini, Q. J. Sattentau, Human immunodeficiency virus type 1
1078 attachment to HeLa CD4 cells is CD4 independent and gp120 dependent and
1079 requires cell surface heparans. *J. Virol.* **72**, 3623–3634 (1998).
1080 118. A. C. S. Saphire, M. D. Bobardt, Z. Zhang, G. David, P. A. Gallay, Syndecans
1081 serve as attachment receptors for human immunodeficiency virus type 1 on
1082 macrophages. *J. Virol.* **75**, 9187–9200 (2001).
1083 119. M. Moulard, *et al.*, Selective interactions of polyanions with basic surfaces on
1084 human immunodeficiency virus type 1 gp120. *J. Virol.* **74**, 1948–1960 (2000).
1085 120. S. Ugolini, I. Mondor, Q. J. Sattentau, HIV-1 attachment: another look. *Trends*
1086 *Microbiol.* **7**, 144–149 (1999).
1087 121. T. M. Dobrowsky, Y. Zhou, S. X. Sun, R. F. Siliciano, D. Wirtz, Monitoring
1088 early fusion dynamics of human immunodeficiency virus type 1 at single-
1089 molecule resolution. *J. Virol.* **82**, 7022–7033 (2008).
1090 122. D. L. Rabenstein, Heparin and heparan sulfate: structure and function. *Nat. Prod.*
1091 *Rep.* **19**, 312–331 (2002).
1092 123. A. Cambi, *et al.*, Microdomains of the C-type lectin DC-SIGN are portals for
1093 virus entry into dendritic cells. *J. Cell Biol.* **164**, 145–155 (2004).
1094 124. L. Wu, V. N. KewalRamani, Dendritic-cell interactions with HIV: infection and
1095 viral dissemination. *Nat. Rev. Immunol.* **6**, 859–868 (2006).
1096

1097

1098 **Figure Legends**

1099

1100 **Figure 1. X4-gp120 modulates CXCR4 dynamics and nanoclustering.** Single-particle
1101 tracking analysis of JKCD4^{+}X4^{-} cells transiently transfected with CXCR4-AcGFP on
1102 fibronectin (FN)-, FN + CXCL12-, or FN + X4-gp120-coated coverslips (828 particles in
1103 96 cells on FN; 2,997 in 95 cells on FN + CXCL12 and 1,547 in 91 cells on FN + X4-
1104 gp120) n = 3. **A)** Percentage of mobile and immobile CXCR4-AcGFP particles at the

1105 membrane of cells treated as indicated. **B)** Diffusion coefficients (D_{1-4}) of mobile
1106 particles at the membrane of cells treated as indicated with the median value of each
1107 experiment (black circles) and the median of all trajectories (dotted black lines). (****p
1108 ≤ 0.0001). **C)** Frequency of CXCR4-AcGFP particles containing monomers and dimers
1109 (≤2) or nanoclusters (≥3), mean ± SD calculated from mean spot intensity (MSI) values
1110 of each particle as compared with the value of monomeric CD86-AcGFP (980 ± 86 a.u.,
1111 **p ≤ 0.01, ***p ≤ 0.001). **D)** Intensity distribution of individual CXCR4-AcGFP
1112 trajectories on unstimulated and CXCL12 or X4-gp120-stimulated cells. Graph shows the
1113 distribution of all trajectories, with the mean value of each experiment (black circles) and
1114 the median of all trajectories (dotted black lines) (n = 3; ****p ≤ 0.0001). Statistical
1115 significance was determined by two-way ANOVA in panels A and C and by non-
1116 parametric Kruskal-Wallis tests followed by Dunn's test for panels B and D.
1117
1118
1119 **Figure 2. gp120-VLPs are mature particles that express a low number of Env**
1120 **trimers. A)** Representative images of clarified VLPs visualized by STED microscopy.
1121 Upper panels show images of the indicated VLPs stained for Gag p24 (blue) and gp120
1122 (red). Lower panels show 10× magnification of equivalent images. White arrows indicate
1123 mature VLPs (p24 condensation). (**B)** Percentage of mature VLPs, analyzed from the
1124 images in A) using TrackAnalyzer in ImageJ, based on p24 intensity and aggregation
1125 level (mean ± SD; n = 2; ****p ≤ 0.0001; the significance indicated on immature VLPs
1126 bar shows the difference with all other conditions). **C)** Percentage of VLPs expressing
1127 gp120 on their surface, as analyzed in ImageJ (mean ± SD; n = 2; ***p ≤ 0.001). **D)**
1128 Distribution of gp120 mean fluorescence intensity. Each spot corresponds to the mean
1129 fluorescence intensity for each analyzed VLP in a.u. The black line represents the mean
1130 of all values (****p ≤ 0.0001). **E)** Frequency of gp120 intensity/particle. Statistical
1131 significance was determined by one-way-ANOVA followed by Tukey's multiple
1132 comparisons test in panels B and C and by Mann-Whitney analysis for panel D.
1133
1134 **Figure 3. gp120 VLPs modulate CXCR4 dynamics and nanoclustering.** Single-
1135 particle tracking analysis of JKCD4$^+$X4$^-$ cells transiently transfected with CXCR4-
1136 AcGFP, on fibronectin (FN)-, FN + VLPs-, or FN + gp120 VLPs-coated coverslips (1,087
1137 particles in 159 cells on FN; 1,400 in 153 cells on FN +VLPs and 1,061 in 160 cells on

1138 FN + gp120 VLPs) n = 6. **A)** Diffusion coefficients ($D_{1–4}$) of mobile particles at the
1139 membrane of cells treated as indicated. Figure shows the mean value of each experiment
1140 (black circles) and the median of all trajectories (dotted black lines) (n = 6; ****p ≤
1141 0.0001). **B)** Frequency of CXCR4-AcGFP particles containing monomers and dimers
1142 (≤2) or nanoclusters (≥3) in cells treated as indicated. Mean ± SD calculated from mean
1143 spot intensity (MSI) values of each particle as compared with the value of monomeric
1144 CD86-AcGFP (980 ± 86 a.u., **p ≤ 0.05, **p ≤ 0.01, ****p ≤ 0.0001). **C)** Intensity
1145 distribution (arbitrary units, a.u.) from individual CXCR4-AcGFP trajectories on cells
1146 treated as indicated. Graph shows the distribution of all trajectories, with the mean value
1147 of each experiment (black circles) and the median of all trajectories (dotted black lines)
1148 (n = 6; ****p ≤ 0.0001). Statistical significance was determined by non-parametric
1149 Kruskal-Wallis tests followed by Dunn's test for panels A and C, and by two-way
1150 ANOVA in panel B.
1151
1152
1153 **Figure 4. gp120 VLPs modulate CXCR4^{R334X} dynamics and nanoclustering.** Single-
1154 particle tracking analysis of JKCD4^{+}X4^{-} cells transiently transfected with CXCR4^{R334X}-
1155 AcGFP, on fibronectin (FN)-, FN + VLPs-, or FN + gp120 VLPs-coated coverslips (341
1156 particles in 63 cells on FN; 610 in 54 cells on FN + VLPs and 707 in 63 cells on FN +
1157 gp120 VLPs) n = 2. **A)** Intensity distribution (arbitrary units, a.u.) from individual
1158 CXCR4^{R334X}-AcGFP trajectories on cells treated as indicated. Graph shows the
1159 distribution of all trajectories, with the mean value of each experiment (black circles) and
1160 the median of all trajectories ± SD (dotted black lines) (n = 2; ****p ≤ 0.0001). **B)**
1161 Diffusion coefficients ($D_{1–4}$) of mobile single particle trajectories at the membrane of cells
1162 treated as indicated. Figure shows the mean value of each experiment (black circles) and
1163 the median of all trajectories (dotted black lines) (n = 2; n.s. not significant, *p ≤ 0.05,
1164 ****p ≤ 0.0001). **C)** Frequency of CXCR4^{R334X}-AcGFP particles containing monomers
1165 plus dimers (≤2) or nanoclusters (≥3), ± SD calculated from mean spot intensity values
1166 of each particle as compared with the value of monomeric CD86-AcGFP (*p ≤ 0.05, ***p
1167 ≤ 0.001). Statistical significance was determined by non-parametric Kruskal-Wallis tests
1168 followed by Dunn's test for panels A and C, and by two-way ANOVA in panel B.
1169
1170

1171 **Figure 5. CD4 forms heterodimers with CXCR4 and CXCR4^{R334X}.** FRET saturation
1172 curves generated using HEK-293T cells transiently transfected with a constant amount of
1173 CD4-CFP DNA (2 μg) and increasing amounts of **A)** CXCR4-YFP (0.5–8.0 μg), **B)**
1174 CXCR4^{R334X}-YFP (0.5–8.0 μg) or **C)** $5HT_{2B}$ DNA (0.5–12 μg). K_D and $FRET_{max}$ values
1175 were calculated using a nonlinear regression equation for a single binding-site model (n
1176 = 2). **D)** FRET efficiency in HEK-293 cells transiently transfected with CXCR4-YFP/
1177 CD4-CFP (ratio 15:9), in the absence or presence of gp120 VLPs or Env(-) VLPs. Data
1178 shows FRET efficiency (arbitrary units, a.u.) (mean ± SD; n = 3; n.s. not significant, *p
1179 ≤ 0.05, ***p ≤ 0.001). **E)** FRET efficiency in HEK-293 cells transiently transfected with
1180 CXCR4^{R334X}-YFP/CD4-CFP (ratio 15:9), in the absence or presence of gp120-VLPs or
1181 Env(-) VLPs. Data shows FRET efficiency (a.u.) (mean ± SD; n = 3; n.s. not significant,
1182 *p ≤ 0.05, ***p ≤ 0.001, ****p ≤ 0.0001). Statistical significance was determined by
1183 unpaired t-test in panels D and E.
1184
1185
1186 **Figure 6. X4-gp120 promote similar internalization patterns of CXCR4 and**
1187 **CXCR4^{R334X} receptors. A)** Surface receptor expression of CXCR4 (white dots) or
1188 CXCR4^{R334X} (black dots), after stimulation with CXCL12 (blue lines) or X4-gp120 (red
1189 lines). Results show mean ± SD of the percentage of receptor expression at the cell surface
1190 (n = 3). **B)** Surface receptor expression of CD4 in JK CD4$^+$ CXCR4$^+$ (white dots) or JK
1191 CD4$^+$ CXCR4^{R334X} (black dots), after stimulation with CXCL12 (blue lines) or X4-gp120
1192 (red lines). Results show mean ± SD of the percentage of receptor expression at the cell
1193 surface (n = 3). Statistical significance was determined by one-way-ANOVA of AUC (*p
1194 ≤ 0.05, **p ≤ 0.01).
1195
1196 **Figure 7. CD4/CXCR4 and CD4/CXCR4^{R334X} complexes support similar HIV-1**
1197 **infection.** The presence of CXCR4^{R334X} on JKCD4$^+$ cells does not alter gp120 binding
1198 and increases fusion events with target cells expressing HIV pHXB2 envelope. **A)**
1199 Binding of X4-gp120 to target cells expressing CD4 and CXCR4 or CD4 and
1200 CXCR4^{R334X} analyzed by flow cytometry. Cells were incubated with 0.3 μg/mL of X4-
1201 gp120 at 37ºC for 30 minutes. Data show MFI (arbitrary units, a.u.) mean ± SD; (n = 2).
1202 Statistical significance was determined using Student's t-test (n.s.= not significant). **B)**
1203 Cell-cell fusion between JKHXBc2-expressing HIV-1 envelope and different target cells
1204 (JKCD4$^+$CXCR4$^+$, JKCD4$^+$CXCR4$^-$ and JKCD4$^+$CXCR4^{R334X}). Prior to co-culture, each

1205 cell type was loaded with the corresponding cell-tracker. Data show the percentage of
1206 fusion events ± SD (n = 6). We used as reference the fusions events detected in
1207 JKCD4^{+}CXCR4^{+} cells (100%). Statistical significance was determined by one-way-
1208 ANOVA (*p < 0.05, ****p ≤ 0.0001). **C**) Representative biparametric histograms from
1209 cells in B showing CMAC *versus* orange fluorophores. **D**) Human PBMCs isolated from
1210 a WHIM patient (WHIM) and three healthy donors (HD1-3) in two independent
1211 experiments were infected with X4-pseudotyped HIV-1_{NL4-3} (MOI: 0.001). At 2 hours
1212 post infection (p.i.), supernatant samples were obtained at different time points (days
1213 post-infection) and p24 levels (pg/mL) in each sample were determined using a
1214 commercial ELISA. Results show mean ± SD (n = 2).
1215
1216
1217 **Video legends**
1218
1219 **Figure 1-video 1** (separate file). Related to Figure 1. Representative video of CXCR4-
1220 AcGFP on live JKCD4^{+}X4^{-} cells treated with DMSO and captured by SPT- TIRF,
1221 showing the diffusion of CXCR4 particles (monomers, dimers, and nanoclusters) at
1222 steady state (FN). The video was acquired and displayed at 10.2 frames/s.
1223
1224 **Figure 1-video 2** (separate file). Related to Figure 1. Representative video of CXCR4-
1225 AcGFP on live JKCD4^{+}X4^{-} cells treated with DMSO and captured by SPT-TIRF,
1226 showing the diffusion of CXCR4 particles (monomers, dimers, and nanoclusters) in
1227 response to CXCL12. The video was acquired and displayed at 10.2 frames/s.
1228
1229 **Figure 1-video 3** (separate file). Related to Figure 1. Representative video of CXCR4-
1230 AcGFP on live JKCD4^{+}X4^{-} cells treated with DMSO and captured by SPT-TIRF,
1231 showing the diffusion of CXCR4 particles (monomers, dimers, and nanoclusters) in
1232 response to X4-gp120. The video was acquired and displayed at 10.2 frames/s.
1233
1234 **Figure 3-video 1** (separate file). Related to Figure 3. Representative video of CXCR4-
1235 AcGFP on live JKCD4^{+}X4^{-} cells treated with DMSO and captured by SPT-TIRF,

1236 showing the diffusion of CXCR4 particles (monomers, dimers, and nanoclusters) at
1237 steady state (FN). The video was acquired and displayed at 10.2 frames/s.

1238

1239 **Figure 3-video 2** (separate file). Related to Figure 3. Representative video of CXCR4-
1240 AcGFP on live JKCD4^{+}X4^{-} cells treated with Env(-) VLPs and captured by SPT-TIRF,
1241 showing the diffusion of CXCR4 particles (monomers, dimers, and nanoclusters) at
1242 steady state (FN). The video was acquired and displayed at 10.2 frames/s.

1243

1244 **Figure 3-video 3** (separate file). Related to Figure 3. Representative video of CXCR4-
1245 AcGFP on live JKCD4^{+}X4^{-} cells treated with gp120 VLPs and captured by SPT-TIRF,
1246 showing the diffusion of CXCR4 particles (monomers, dimers, and nanoclusters) at
1247 steady state (FN). The video was acquired and displayed at 10.2 frames/s.

1248

1249 **Figure 4-video 1** (separate file). Related to Figure 4. Representative video of
1250 CXCR4R334X-AcGFP on live JKCD4^{+}X4^{-} cells treated with DMSO and captured by
1251 SPT-TIRF, showing the diffusion of CXCR4 particles (monomers, dimers, and
1252 nanoclusters) at steady state (FN). The video was acquired and displayed at 10.2 frames/s.
1253

1254 **Figure 4-video 2** (separate file). Related to Figure 4. Representative video of
1255 CXCR4R334X-AcGFP on live JKCD4^{+}X4^{-} cells treated with Env(-) VLPs and captured
1256 by SPT-TIRF, showing the diffusion of CXCR4 particles (monomers, dimers, and
1257 nanoclusters) at steady state (FN). The video was acquired and displayed at 10.2 frames/s.
1258

1259 **Figure 4-video 3** (separate file). Related to Figure 4. Representative video of
1260 CXCR4R334X-AcGFP on live JKCD4^{+}X4^{-} cells treated with gp120 VLPs and captured
1261 by SPT-TIRF, showing the diffusion of CXCR4 particles (monomers, dimers, and
1262 nanoclusters) at steady state (FN). The video was acquired and displayed at 10.2 frames/s.
1263

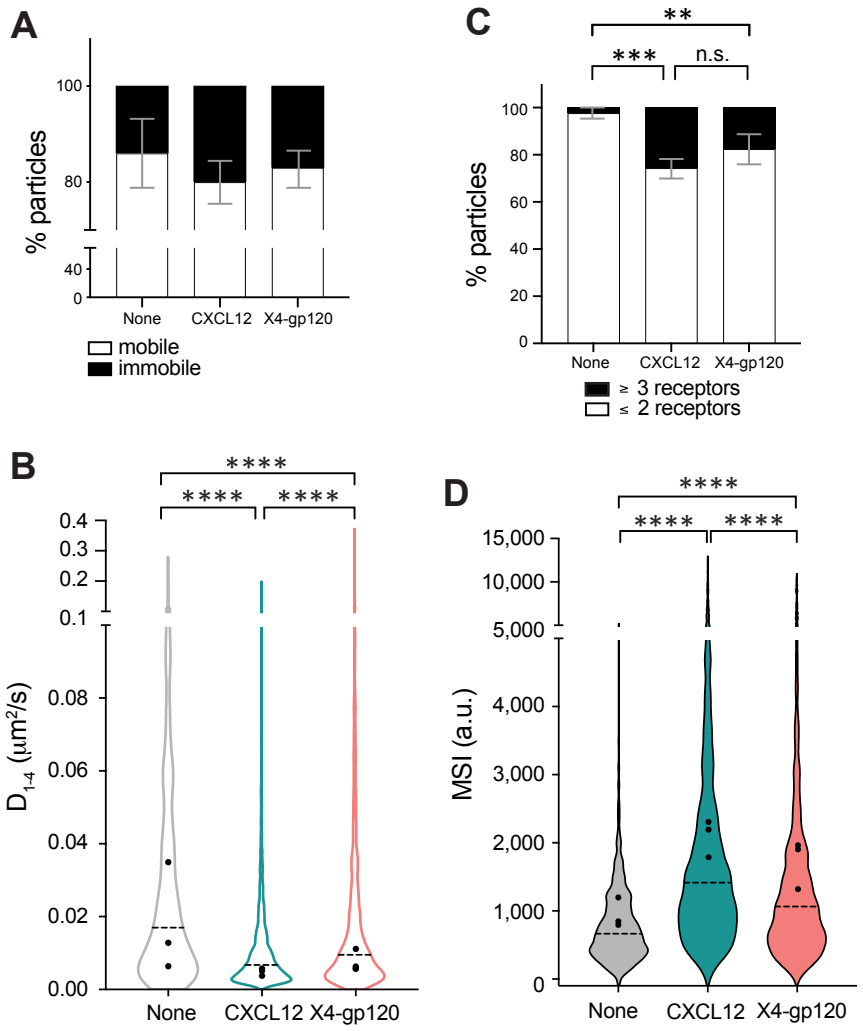
A
% particles
100
80
40
0
None
CXCL12
X4-gp120
mobile
immobile
C
**
***
n.s.
% particles
100
80
60
40
20
0
None
CXCL12
X4-gp120
≥ 3 receptors
≤ 2 receptors
B
****
****
****
D_{1-4} (µm²/s)
0.4
0.3
0.2
0.1
0.08
0.06
0.04
0.02
0.00
None
CXCL12
X4-gp120
D
****
****
****
MSI (a.u.)
15,000
10,000
5,000
4,000
3,000
2,000
1,000
0
None
CXCL12
X4-gp120

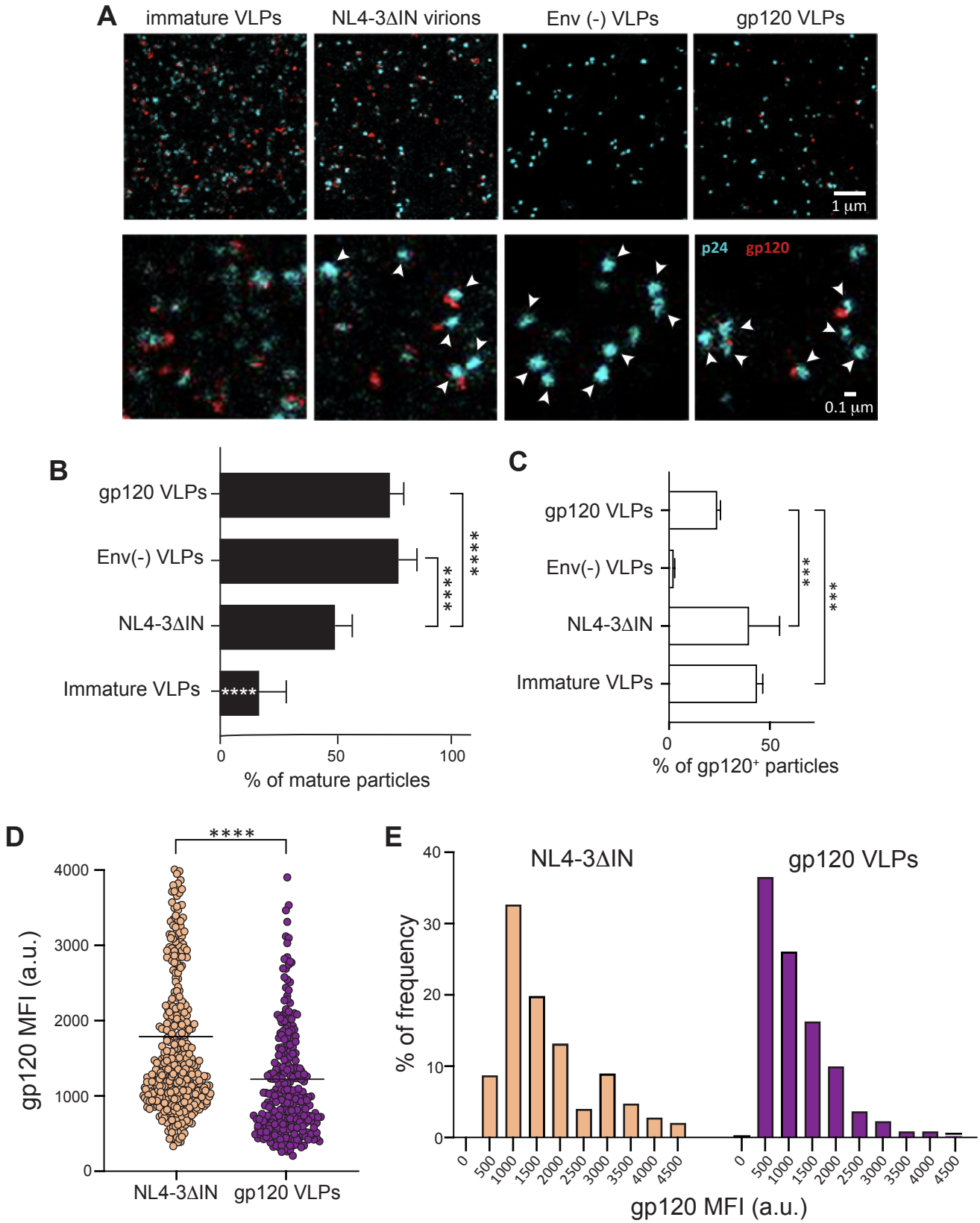
A
immature VLPs
NL4-3ΔIN virions
Env (-) VLPs
gp120 VLPs
1 µm
p24
gp120
0.1 µm
B
gp120 VLPs
Env(-) VLPs
NL4-3ΔIN
Immature VLPs
****
0
50
100
% of mature particles
C
gp120 VLPs
Env(-) VLPs
NL4-3ΔIN
Immature VLPs
***
0
50
% of gp120⁺ particles
D
****
gp120 MFI (a.u.)
4000
3000
2000
1000
0
NL4-3ΔIN
gp120 VLPs
E
NL4-3ΔIN
gp120 VLPs
% of frequency
40
30
20
10
0
0
500
1000
1500
2000
2500
3000
3500
4000
4500
gp120 MFI (a.u.)

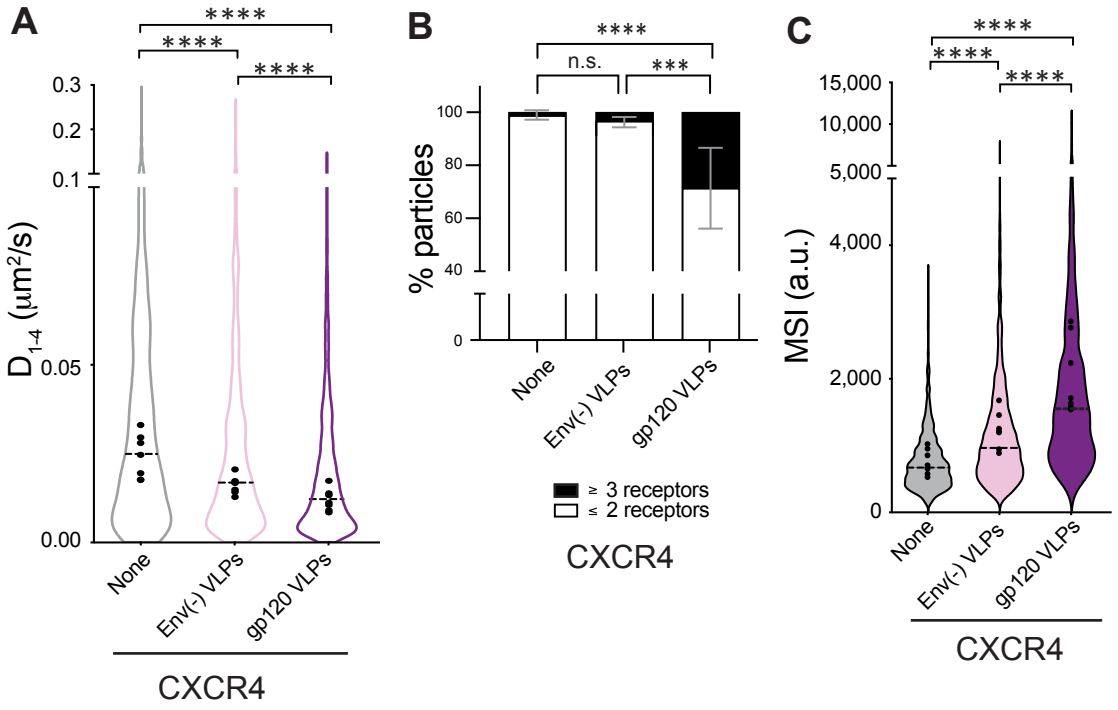
A
****
****
****
0.3
0.2
0.1
0.05
0.00
D1-4 (µm2/s)
None
Env(-) VLPs
gp120 VLPs
CXCR4
B
****
n.s.
***
100
80
60
40
0
% particles
None
Env(-) VLPs
gp120 VLPs
≥ 3 receptors
≤ 2 receptors
CXCR4
C
****
****
****
15,000
10,000
5,000
4,000
2,000
0
MSI (a.u.)
None
Env(-) VLPs
gp120 VLPs
CXCR4

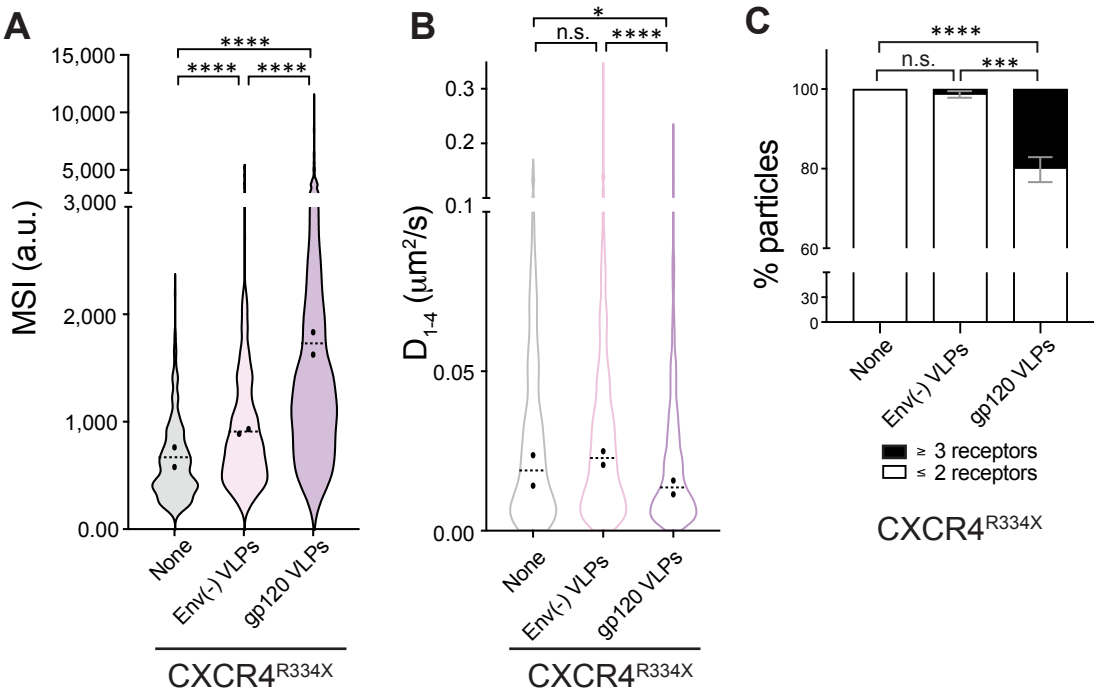
A
MSI (a.u.)
15,000
10,000
5,000
3,000
2,000
1,000
0.00
****
****
****
None
Env(-) VLPs
gp120 VLPs
CXCR4R334X
B
D1-4 (µm2/s)
0.3
0.2
0.1
0.05
0.00
*
n.s.
****
None
Env(-) VLPs
gp120 VLPs
CXCR4R334X
C
% particles
100
80
60
30
0
****
n.s.
***
None
Env(-) VLPs
gp120 VLPs
≥ 3 receptors
≤ 2 receptors
CXCR4R334X

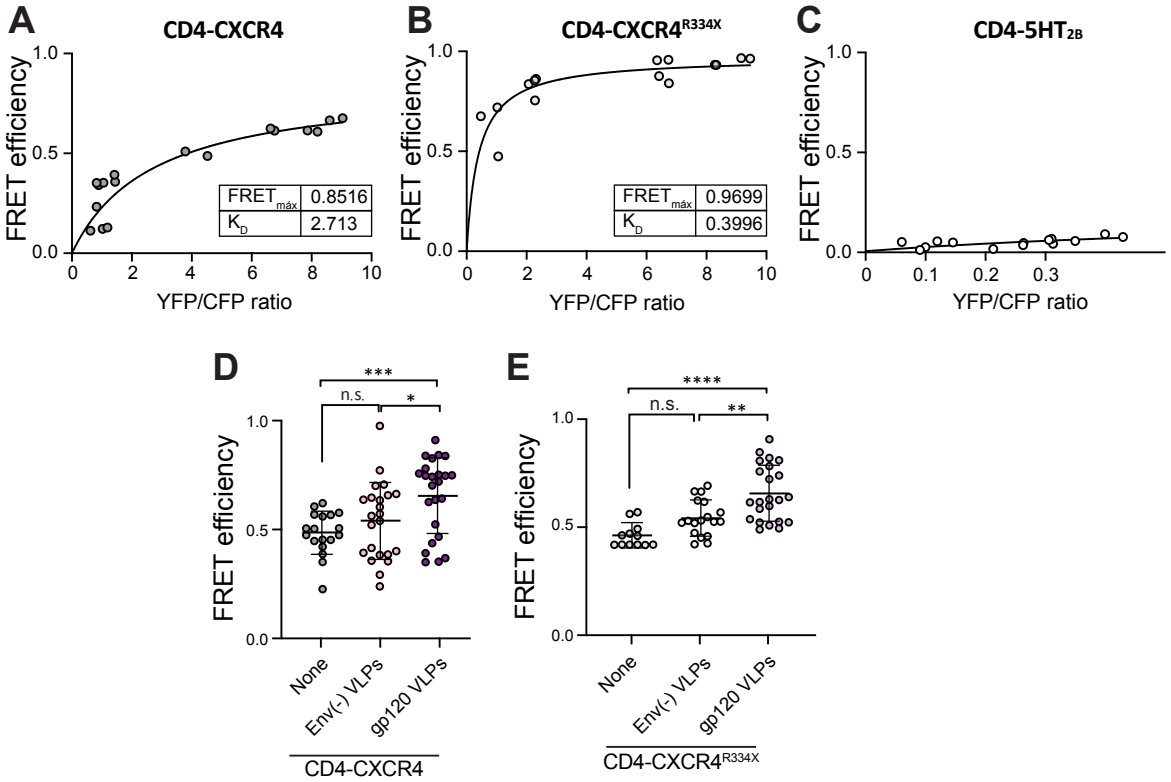
A
CD4-CXCR4
FRET efficiency
YFP/CFP ratio
FRETmáx 0.8516
KD 2.713
B
CD4-CXCR4R334X
FRET efficiency
YFP/CFP ratio
FRETmáx 0.9699
KD 0.3996
C
CD4-5HT2B
FRET efficiency
YFP/CFP ratio
D
FRET efficiency
***
n.s.
*
None
Env(-) VLPs
gp120 VLPs
CD4-CXCR4
E
FRET efficiency
****
n.s.
**
None
Env(-) VLPs
gp120 VLPs
CD4-CXCR4R334X

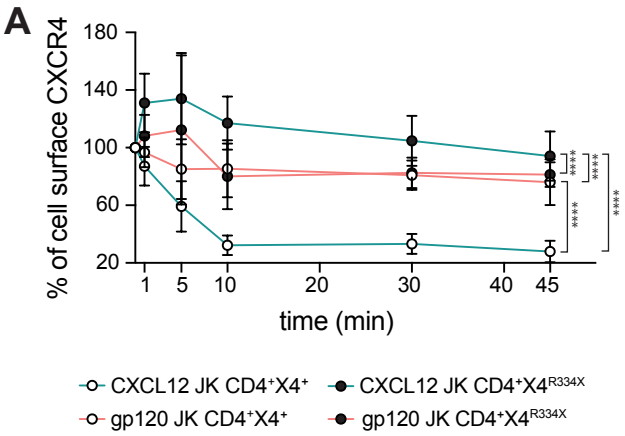
A
% of cell surface CXCR4
180
140
100
60
20
1
5
10
20
30
40
45
time (min)
****
****
****
****
CXCL12 JK CD4+X4+
CXCL12 JK CD4+X4R334X
gp120 JK CD4+X4+
gp120 JK CD4+X4R334X

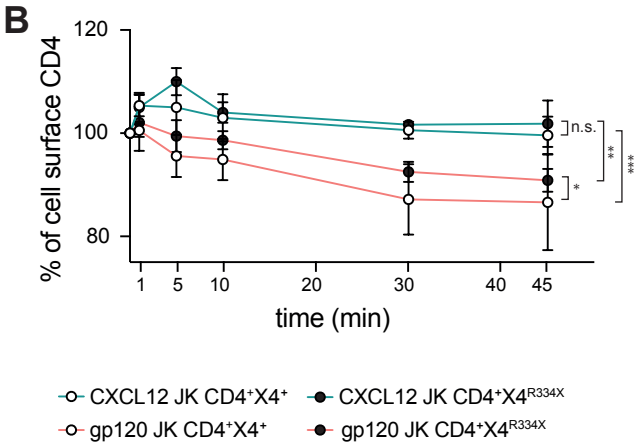
B
% of cell surface CD4
120
100
80
1
5
10
20
30
40
45
time (min)
n.s.
*
**
***
CXCL12 JK CD4+X4+
CXCL12 JK CD4+X4R334X
gp120 JK CD4+X4+
gp120 JK CD4+X4R334X

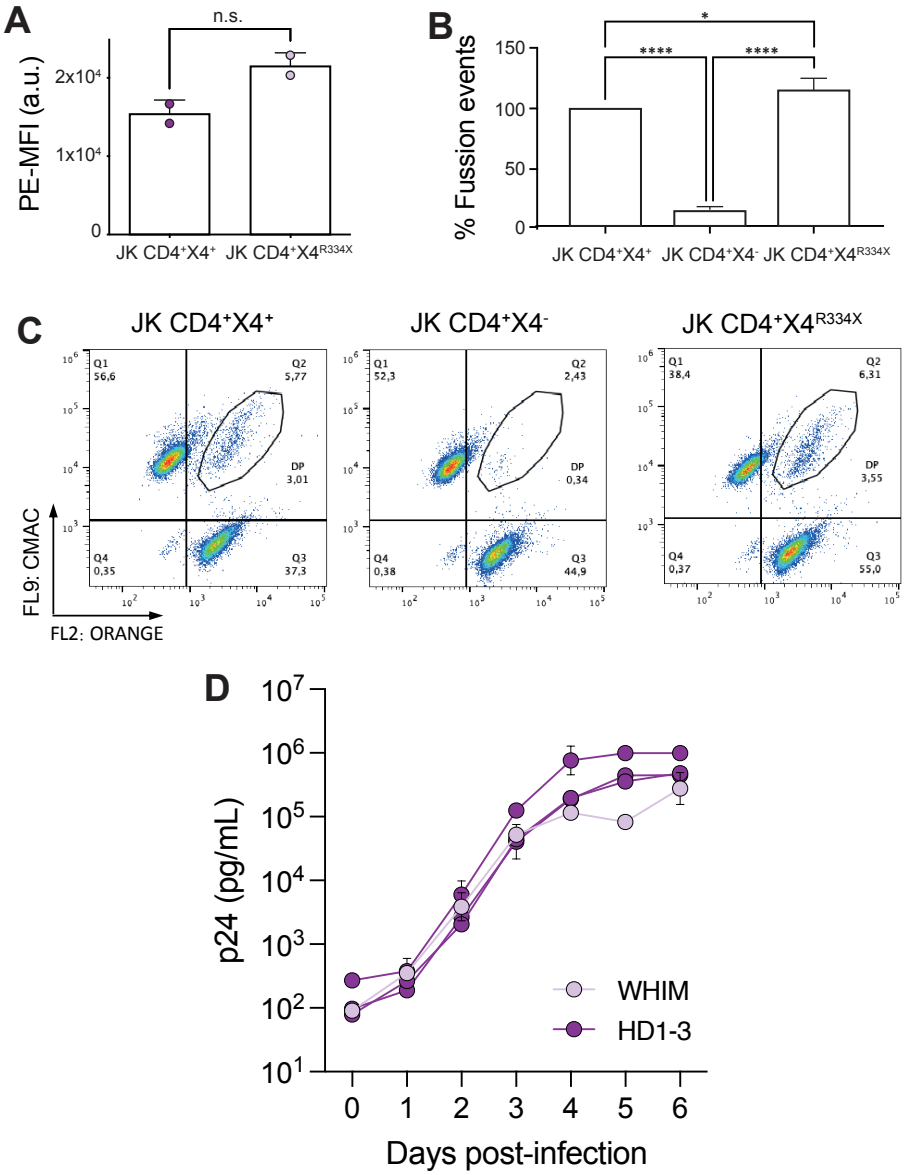
A
n.s.
PE-MFI (a.u.)
2x10⁴
1x10⁴
0
JK CD4⁺X4⁺
JK CD4⁺X4R334X
B
*
****
****
% Fussion events
150
100
50
0
JK CD4⁺X4⁺
JK CD4⁺X4⁻
JK CD4⁺X4R334X
C
JK CD4⁺X4⁺
JK CD4⁺X4⁻
JK CD4⁺X4R334X
Q1 56,6
Q2 5,77
DP 3,01
Q4 0,35
Q3 37,3
Q1 52,3
Q2 2,43
DP 0,34
Q4 0,38
Q3 44,9
Q1 38,4
Q2 6,31
DP 3,55
Q4 0,37
Q3 55,0
FL9: CMAC
FL2: ORANGE
D
p24 (pg/mL)
10⁷
10⁶
10⁵
10⁴
10³
10²
10¹
0
1
2
3
4
5
6
Days post-infection
WHIM
HD1-3

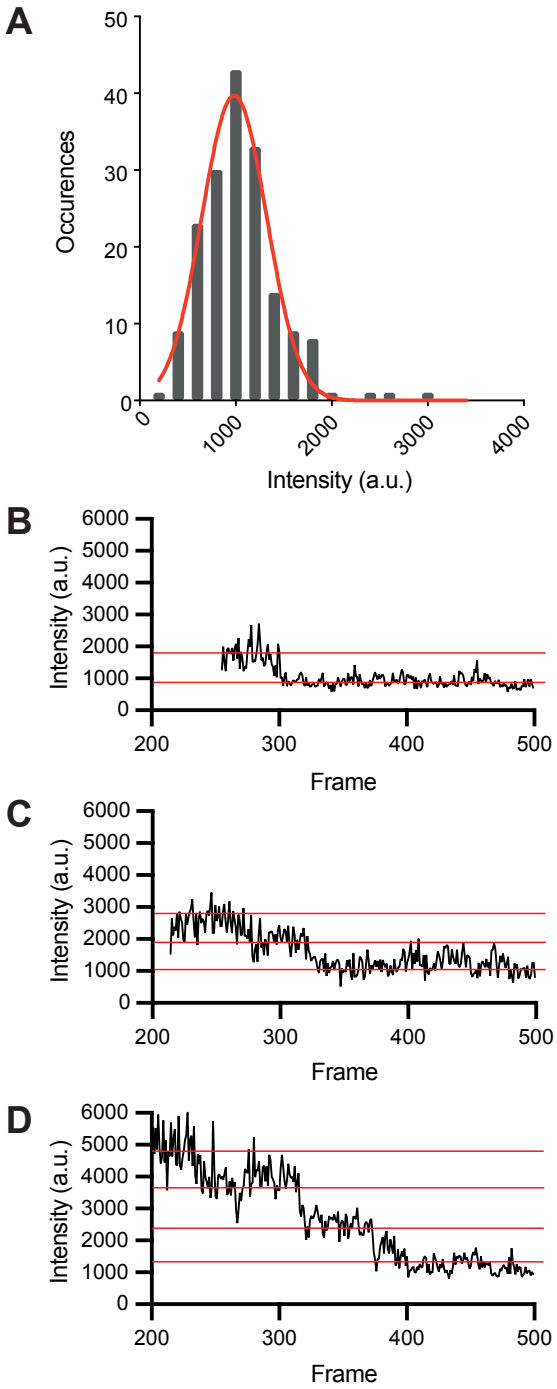

Figure 1-Figure supplement 1. Characterization and calculation of reference parameters for particles intensity, related to TIRF images. A) Fluorescence intensity histogram from monomeric CD86-AcGFP single particles, detected by one photobleaching step evaluation (data from 118 trajectories in 21 cells in 3 separate experiments). The reference fluorescence intensity value for monomer (980 ± 86 a.u.) was obtained from the Gaussian fit (red line) of the histogram. Representative graphics of one-step **(B),** two-step **(C)** and three-step photobleaching **(D)** of the monomeric CXCR4-AcGFP particle.

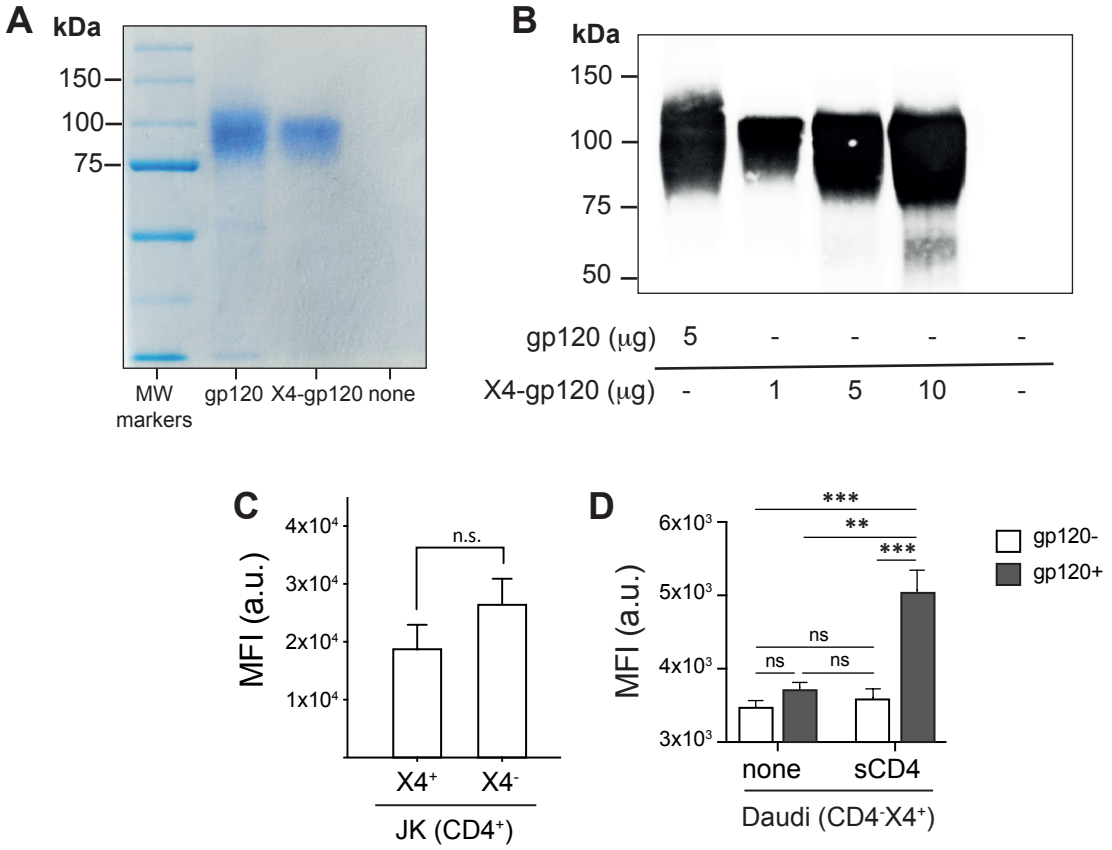

Figure 1-Figure supplement 2. Generation of functional recombinant X4-gp120. A) Representative Coomassie blue-stained polyacrylamide gel of 5 μg of purified recombinant X4-gp120 and commercial gp120 (gp120), used as a control (n = 3). **B)** Representative western blot of different amounts (μg indicated) of recombinant X4-gp120 and commercial gp120 (5 μg), used as control, analyzed with an anti-gp120 mAb (n = 3). **C)** Flow cytometry of X4-gp120 binding to JKCD4+CXCR4+ (JKCD4+X4+) and JKCD4+CXCR4- (JKCD4+X4-) cells analyzed with an anti-Histidine mAb. Mean MFI values (and SD) are shown (n = 3; n.s. = not significant). **D)** Flow cytometry of X4-gp120 binding on Daudi cells (CD4-X4+), pretreated or not with soluble recombinant human CD4 (sCD4), analyzed with an anti-His mAb. As control the binding of sCD4 in the absence of X4-gp120 is also shown. Mean MFI values (and SD) are shown (n = 3; **p ≤ 0.01). Statistical significance was determined by paired t-test for panel C, and by two-way ANOVA in panel B.

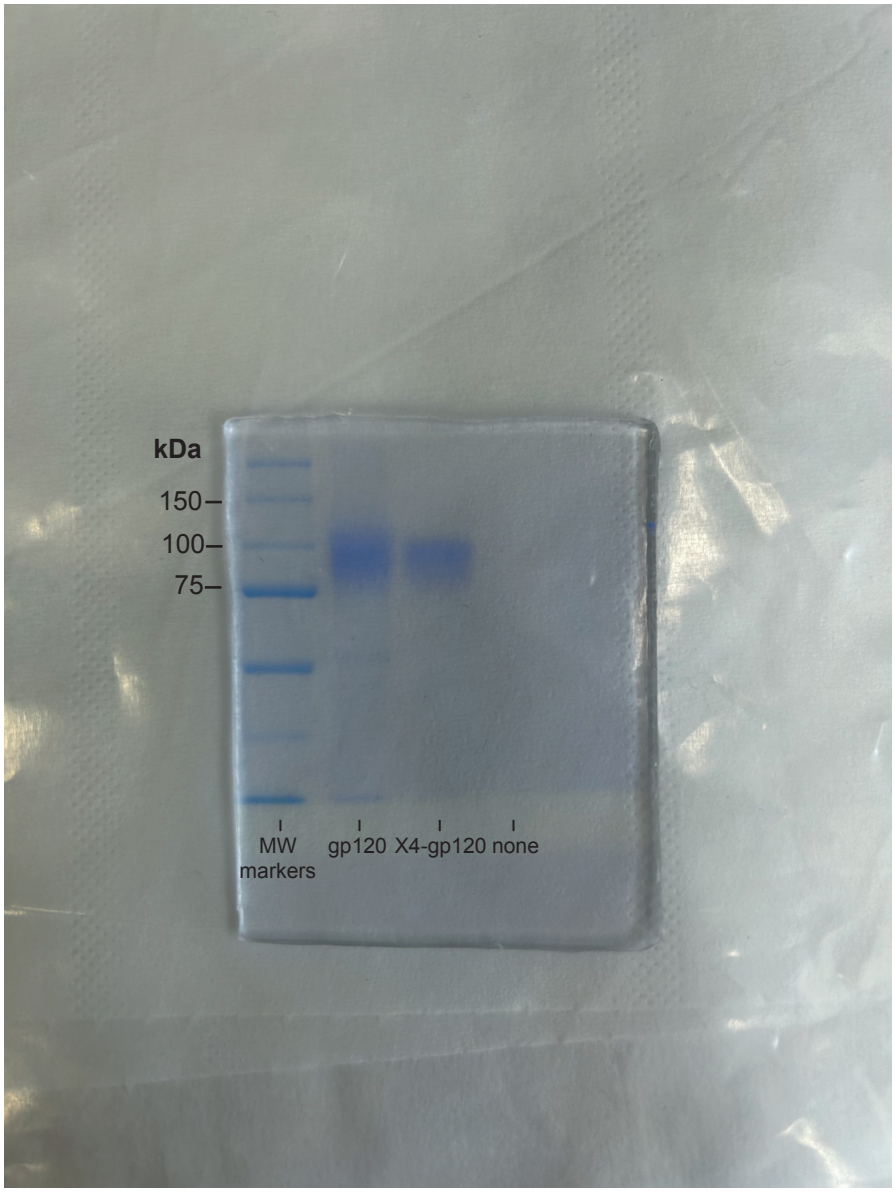

Figure 1-Figure supplement 2-Source Data 1. Generation of functional recombinant X4-gp120. Coomassie blue-stained polyacrylamide gel of 5 μg of purified recombinant X4-gp120 and commercial gp120 (gp120), used as a control.

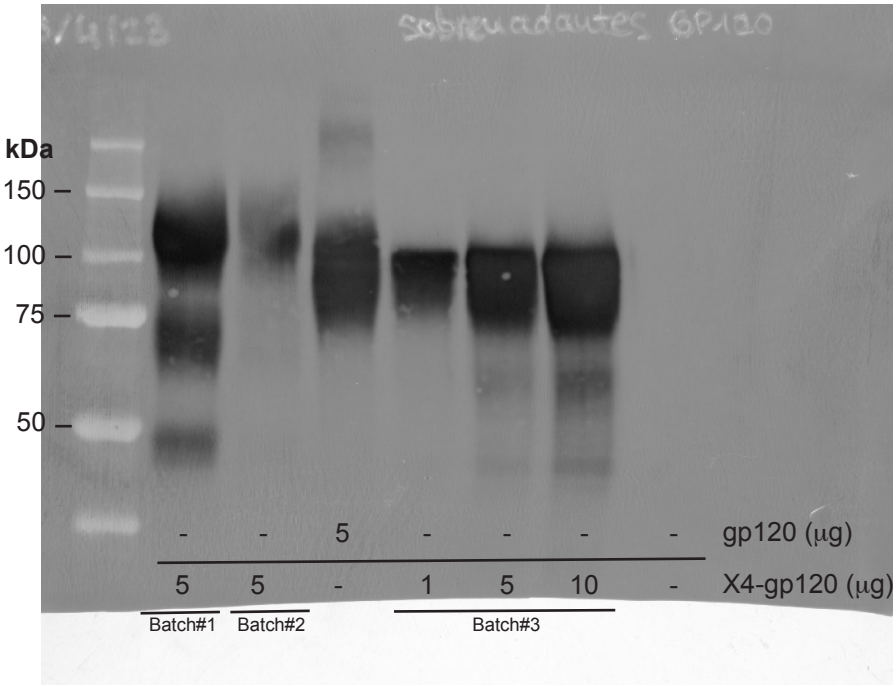

Figure 1-Figure supplement 2-Source data 2. Original membrane corresponding to Figure 1-Figure supplement 2, panel B. Western blot of different amounts (μg indicated) of different batches of recombinant X4-gp120 and commercial gp120 (5 μg), used as control, analyzed with an anti-gp120 mAb. Batch#3 was selected for further assays.

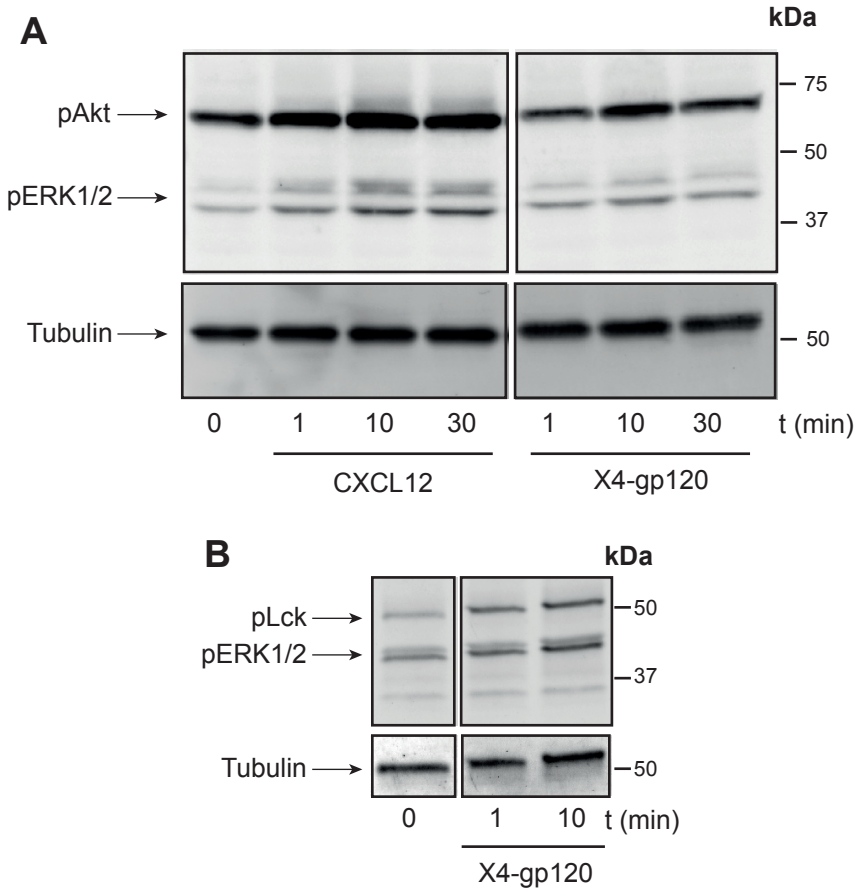

Figure 1-Figure supplement 3. X4-gp120 activates CD4- and CXCR4-related signaling pathways in target cells. A) Western blot of lysed Jurkat cells activated with CXCL12 (50 nM) or X4-gp120 at the indicated time points and analyzed with anti-pAkt and pERK1/2 antibodies. A representative membrane is shown (n = 3). **B)** Western blot of primary $CD4^+$ T blast lysates activated with X4-gp120 at the indicated time points and analyzed using anti-pLck and -pERK1/2 antibodies. A representative membrane is shown (n = 3). In both cases, membranes were reblotted with an anti-tubulin mAb as a loading control. Molecular markers (kDa) are also shown.

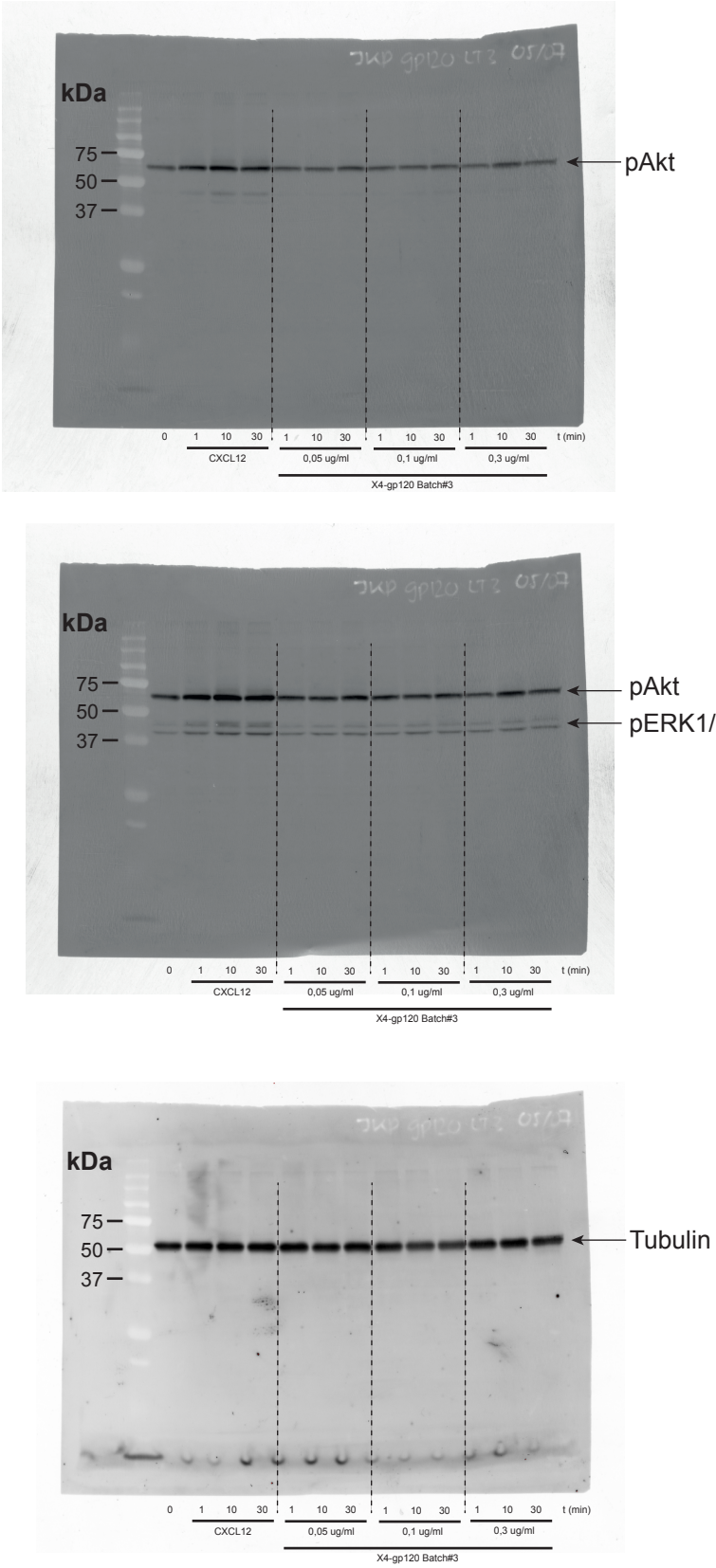

Figure 1-Figure supplement 3-Source data 1. Original membrane corresponding to Figure 1-Figure supplement 3, panel A. Western blot of lysed Jurkat cells activated with CXCL12 (50 nM) or X4-gp120 Batch#3 (0.05; 0.1; 0.3 ug/ml) at the indicated time points and analyzed with anti-pAkt and pERK1/2 antibodies. Membrane were reblotted with an anti-tubulin mAb as a loading control. Molecular markers (kDa) are also shown. Figure 1-Figure supplement 3, panel A shows western blot of lysed Jurkat cells activated with CXCL12 (50 nM) and X4-gp120 Batch#3 0.3 ug/ml.

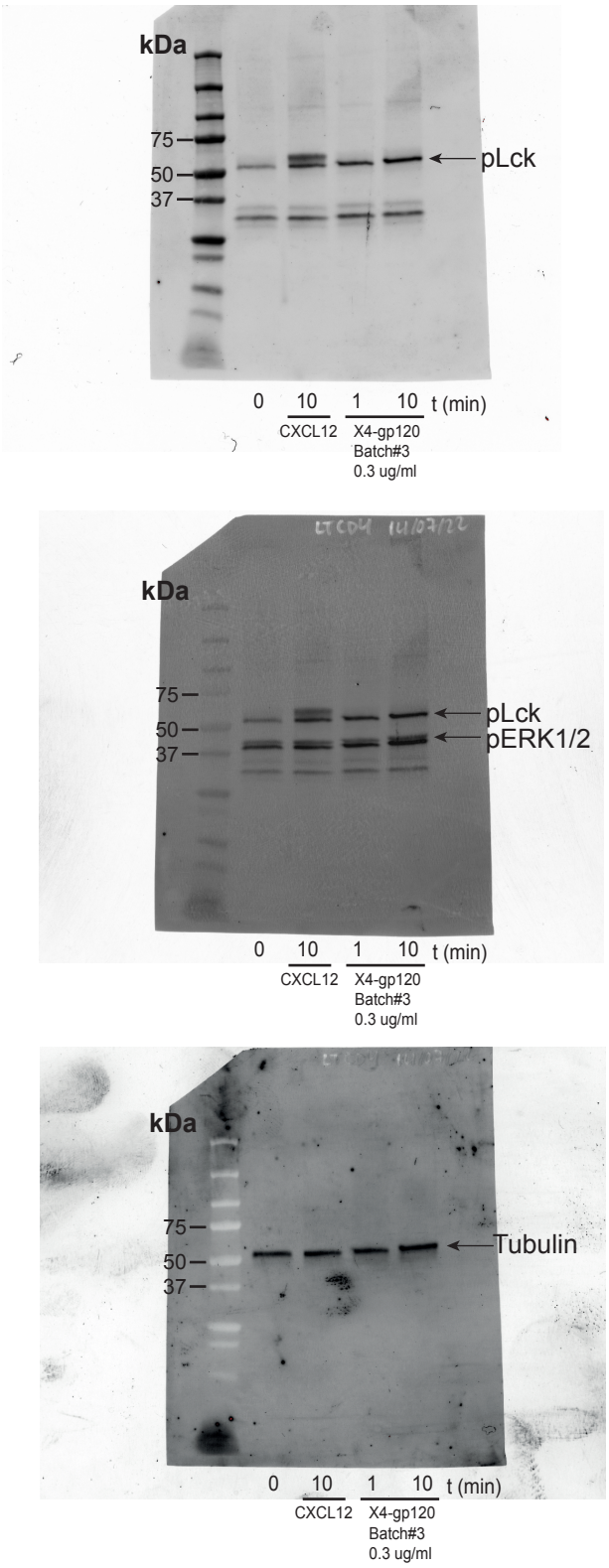

Figure 1-Figure supplement 3-Source data 2. Original membrane corresponding to Figure 1-Figure supplement 3, panel B. Western blot of primary CD4$^+$ T blast lysates activated with CXCL12 (50nM) and X4-gp120 Batch#3 (0.3 ug/ml) at the indicated time points and analyzed using anti-pLck and -pERK1/2 antibodies. Membrane were reblotted with an anti-tubulin mAb as a loading control. Molecular markers (kDa) are also shown. Figure 1-Figure supplement 3, panel B shows western blot of lysed Jurkat cells activated with X4-gp120 Batch#3 0.3 ug/ml.

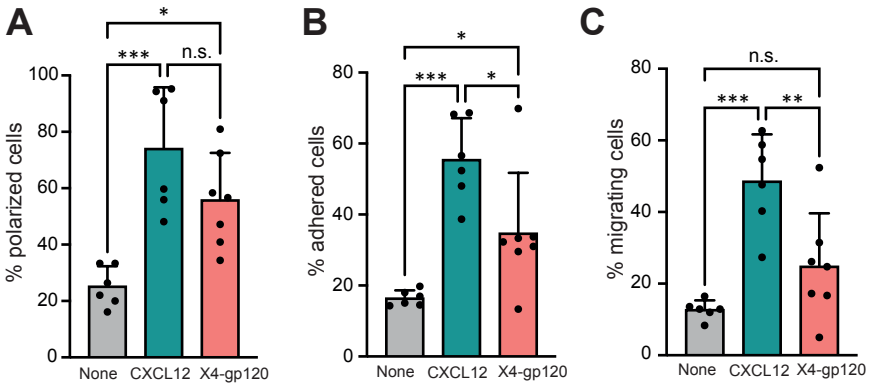

Figure 1-Figure supplement 4. X4-gp120 induces cell polarization. A) CD4+ T cell blasts were perfused in flow chambers coated with ICAM-1-containing lipid bilayers, alone or with CXCL12- or X4-gp120. Polarized cells were determined from differential interference contrast (DIC) images using ImageJ2 and Imaris 7.0 and expressed as a percentage of the total number of cells per image (mean ± SD with the mean value of each experiment (black circles) indicated; n = 6; n.s. not significant; *p ≤ 0.05; ***p ≤ 0.001). **B)** Cells were perfused as in A) and the percentage of adhered cells was determined using the interference reflection microscopy (IRM) signal. The frequency of adhesion (IRM^+ cells) per image field was estimated as [nº of cells showing IRM contact/total nº of cells (estimated by DIC)] × 100. More than 150 cells were analyzed of each condition. Data are shown as percentage of adhered cells. (Mean ± SD with the mean value of each experiment (black circles) indicated; n = 6; *p ≤ 0.05; ***p ≤ 0.001). **C)** Cells in B were analyzed for cell migration. We calculated the frequency of migration (cells showing an IRM^+ contact and moving over time). Data are presented as percentage of migrating cells (mean ± SD with the mean value of each experiment (black circles) indicated; n = 6; n.s. = not significant; **p ≤ 0.01; *** p ≤ 0.001). Statistical significance was determined by one-way ANOVA followed by Tukey's multiple comparisons test for all panels.

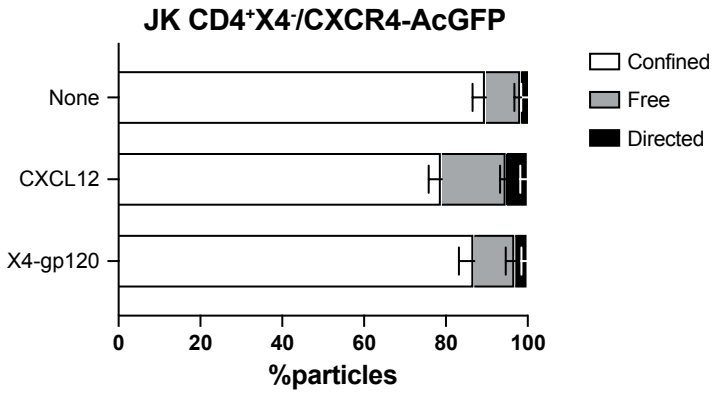

Figure 1-Figure supplement 5. Classification of mobile receptor trajectories. Percentage of mobile receptor trajectories classified as confined, free or directed for JK $CD4^+X4^-$ cells transiently transfected with CXCR4-AcGFP in steady state or after CXCL12 or X4-gp120 stimulation. Statistical significance was determined by two-way ANOVA test.

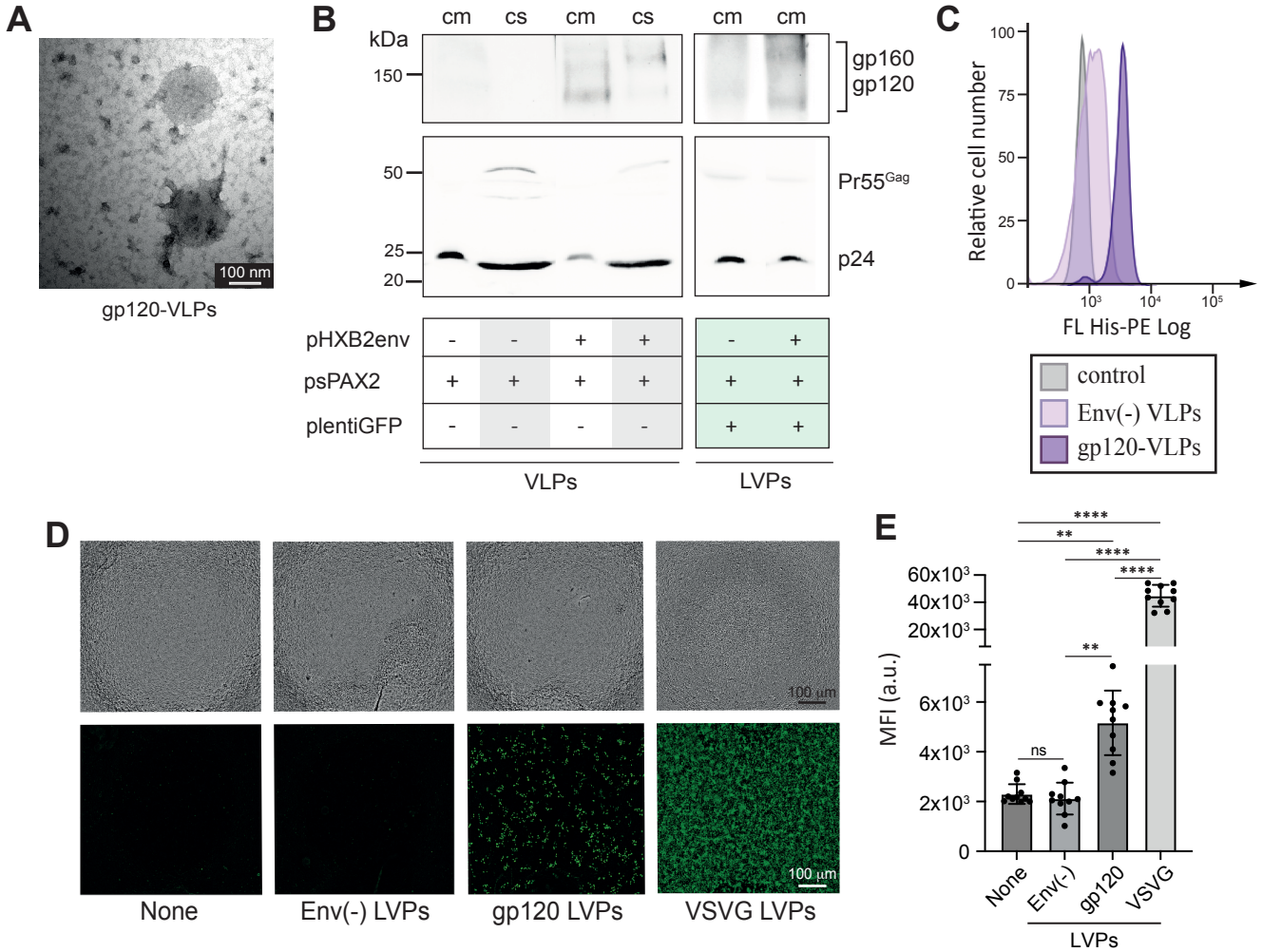

Figure 2-Figure supplement 1. Characterization of gp120-VLPs and LVPs. A) Representative transmission electron micrographs of gp120-VLP particles. Original scale bar 100 nm. **B)** Culture media of transfected HEK-293T cells (cm) with different constructs, as indicated, and the corresponding clarified samples (cs) containing the VLPs or the LVPs generated, were analyzed by western blot with anti-p24, and -gp120 mAbs. The anti-p24 mAb also recognizes $Pr55^{Gag}$, a precursor of p24 presents in immature particles. Molecular weight markers are indicated (kDa). **C)** Flow cytometry analysis of VLPs (Env(-) and expressing x4-gp120) bound to latex beads in the presence of soluble human CD4, using an anti-Histidine mAb. A representative experiment is shown of 3 performed. **D)** Representative transduction experiments using the indicated LVPs, where the reporter expression was captured using the Tecan SparkCyto reader. Upper panels show bright-field images of target HEK-293 CD4 cells. Lower panels show fluorescence signal from GFP expression in transduced cells. Images were captured with a 4× objective, using an exposure of 200 ms in all cases and 80 ms for control VSVG-VLPs (positive control). Env(-) LVPs were used as negative control (n = 3). **E)** Quantification of the Mean Fluorescence Intensity (MFI) of images obtained in transduction experiments

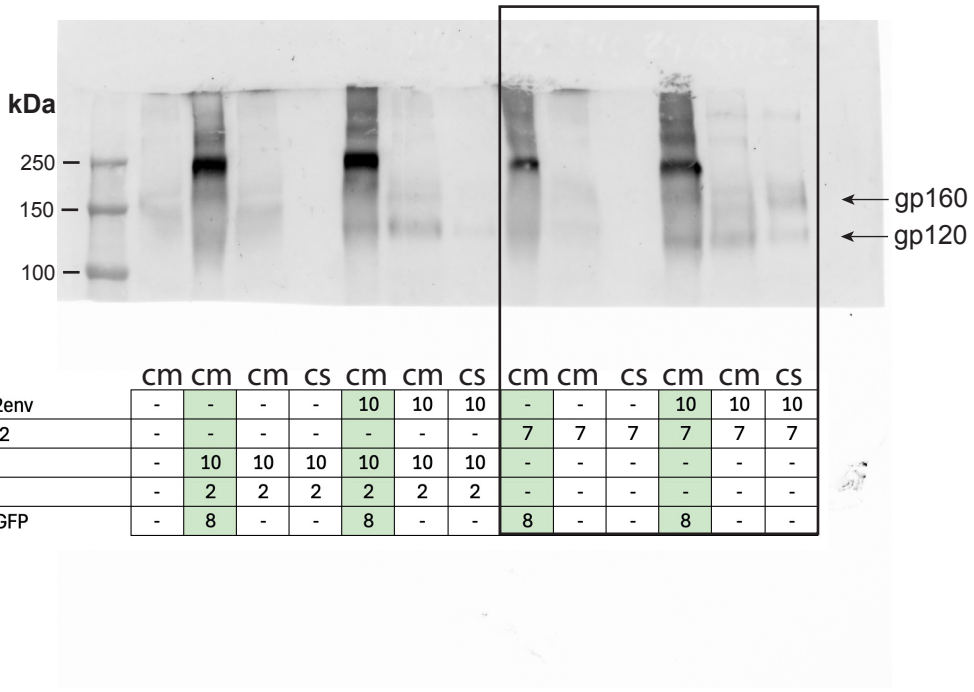

	cm	cm	cm	cs	cm	cm	cs	cm	cm	cs	cm	cm	cs
pHXB2env	-	-	-	-	10	10	10	-	-	-	10	10	10
psPAX2	-	-	-	-	-	-	-	7	7	7	7	7	7
pRRE	-	10	10	10	10	10	10	-	-	-	-	-	-
Rev	-	2	2	2	2	2	2	-	-	-	-	-	-
plentiGFP	-	8	-	-	8	-	-	8	-	-	8	-	-

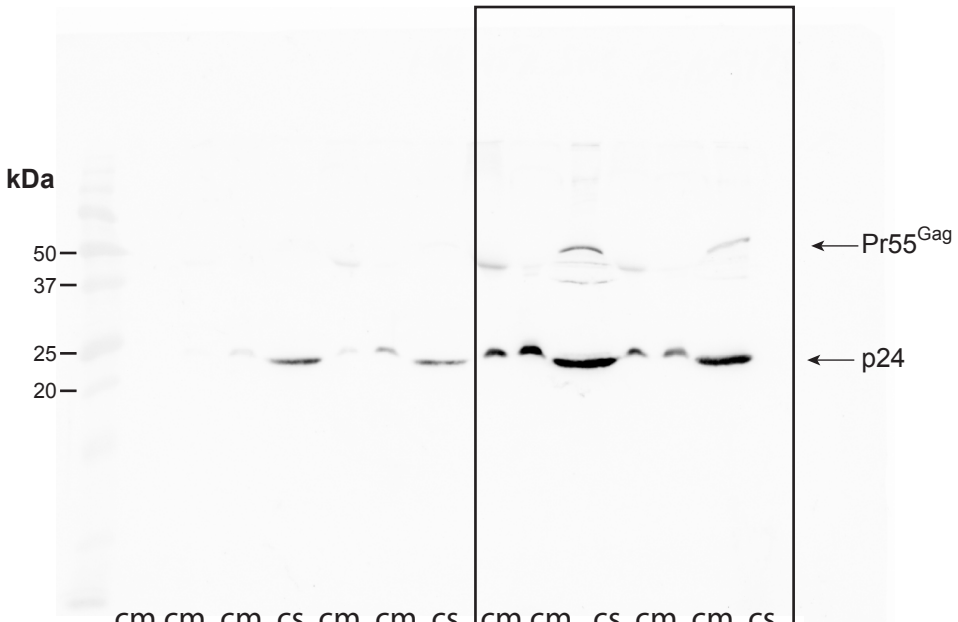

	cm	cm	cm	cs	cm	cm	cs	cm	cm	cs	cm	cm	cs
pHXB2env	-	-	-	-	10	10	10	-	-	-	10	10	10
psPAX2	-	-	-	-	-	-	-	7	7	7	7	7	7
pRRE	-	10	10	10	10	10	10	-	-	-	-	-	-
Rev	-	2	2	2	2	2	2	-	-	-	-	-	-
plentiGFP	-	8	-	-	8	-	-	8	-	-	8	-	-

cm (culture media)
cs (clarified simples dil 1/25)

LVPs | VLPs

Figure 2-Figure supplement 1-Source data 1. Original membranes corresponding to Figure 2-Figure supplement 1, panel B. Culture media of transfected HEK-293T cells (cm) with different constructs, as indicated, and the corresponding clarified samples (cs) containing the VLPs or the LVPs generated, were analyzed by western blot with anti-p24, and -gp120 mAbs. The anti-p24 mAb also recognizes $Pr55^{Gag}$, a precursor of p24 presents in immature particles. Molecular weight markers are indicated (kDa). Figure 2-Figure supplement 1, panel B shows the last six lanes of these membranes reorganized to separate LVPs from VLPs.

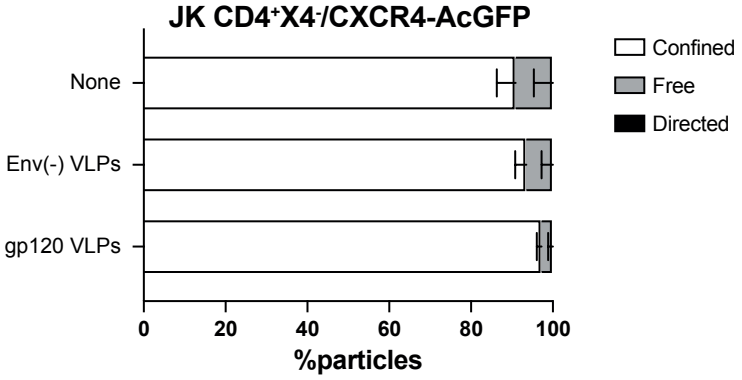

Figure 3-Figure supplement 1. Classification of mobile receptor trajectories. Percentage of mobile receptor trajectories classified as confined, free or directed for JK $CD4^+X4^-$ cells transiently transfected with CXCR4-AcGFP in steady state or after Env(-) VLPs or gp120 VLPs stimulation. Statistical significance was determined by two-way ANOVA test.

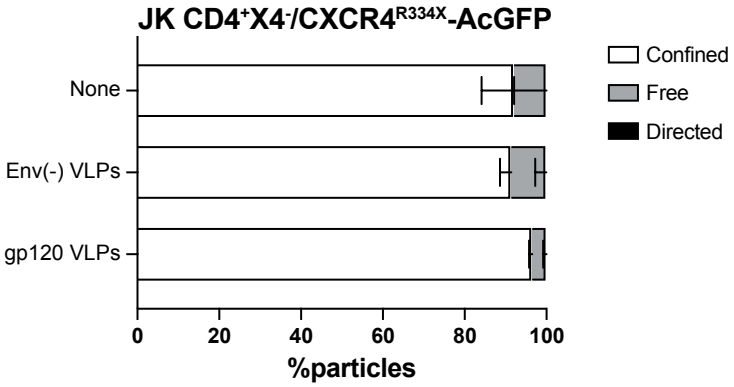

Figure 4-Figure supplement 1. Classification of mobile receptor trajectories. Percentage of mobile receptor trajectories classified as confined, free or directed for JK $CD4^{+}X4^{-}$ cells transiently transfected with $CXCR4^{R334X}$-AcGFP in steady state or after Env(-) VLPs or gp120 VLPs stimulation. Statistical significance was determined by two-way ANOVA test.

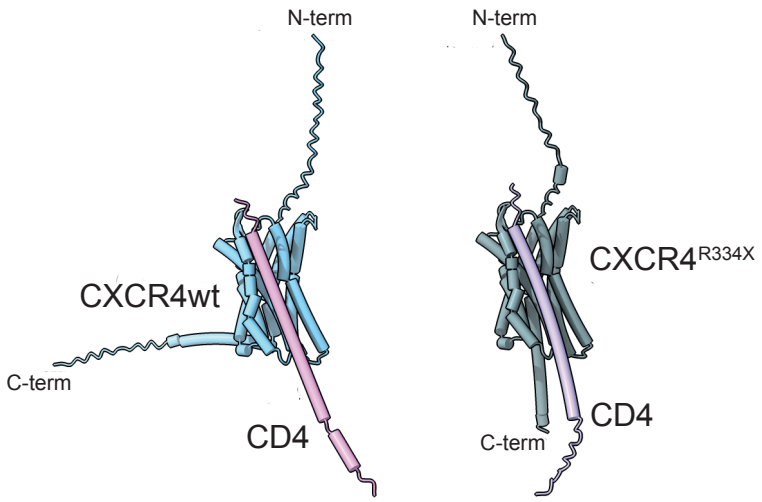

Figure 5-Figure supplement 1. Predicted interaction between CD4 and CXCR4 or CXCR4R334X by AlphaFold3. Predicted interactions between CD4 transmembrane and cytoplasmic domain (residues 361-433) and CXCR4 (left panel) or CXCR4R334X (right panel) at 1:1 ratio.

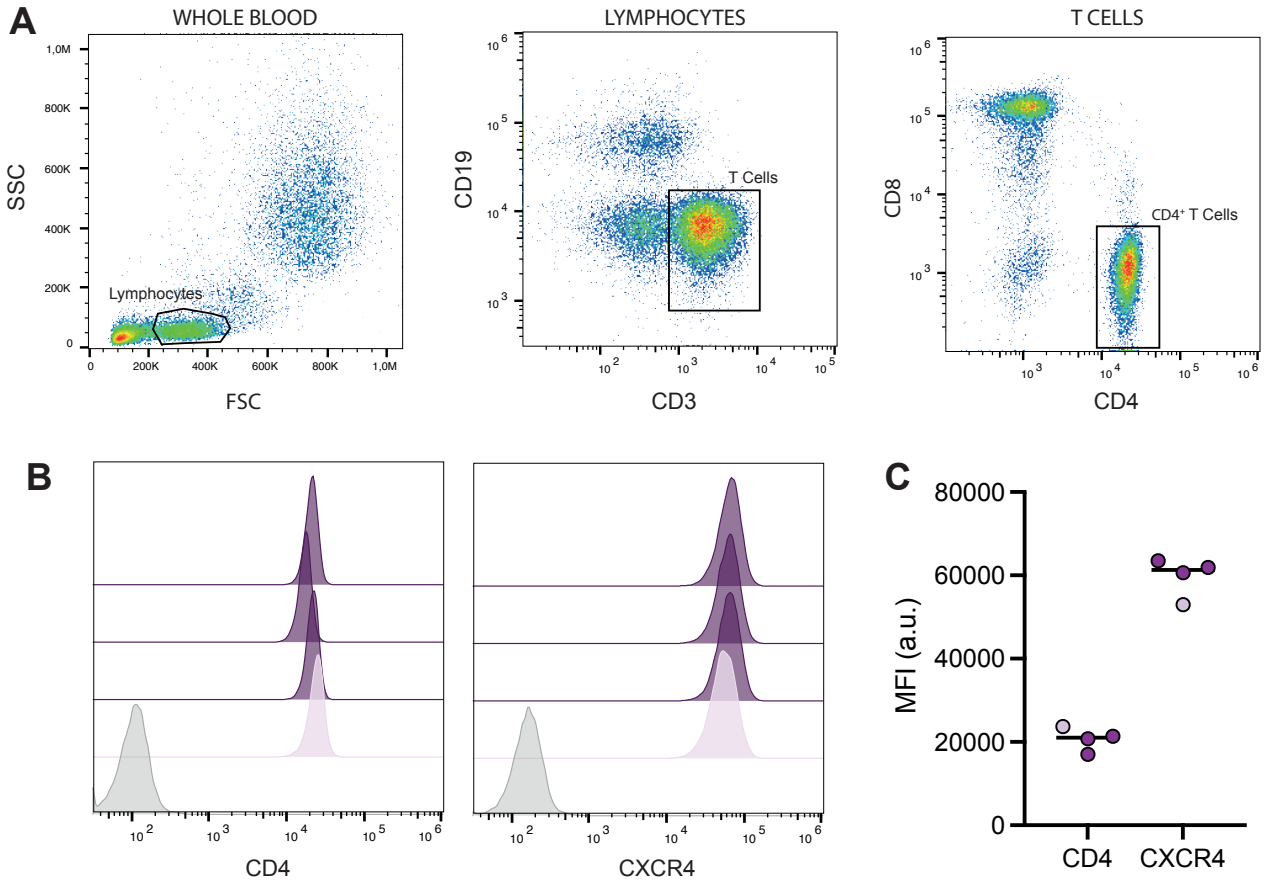

Figure 7-Figure supplement 1. Characterization of CD4+ T cell populations in blood from healthy controls and a WHIM patient. A) Gating strategy and **B)** analysis of CD4 and CXCR4 expression on CD4+T cells. **C)** Mean fluorescence intensity (MFI) of CD4 and CXCR4 on CD4+T cells from samples in A.